Abstract

Medical Technology

SCHEDULE

Morning Session : 11:00 ~ 12:00

Session chair: Prof. Tsutomu Kawabe

1. Cancer-directed delivery of doxorubicin-rapamycin and cancer imaging by anti-Her2 immunoliposomes — Min Woo Kim
2. Variation of IgE-binding epitopes in the allergen after repeated immunization — Takehiro Yamaguchi
3. Evaluation of human papillomavirus oncogenic mRNA testing for diagnosis of cervical cancer by using real-time NASBA — Geehyuk Kim

Afternoon Session : 13:30 ~ 16:00

Session chair: Prof. Takaaki Kondo

4. Quantitation of neonicotinoid metabolites in human urine using gas chromatography-mass spectrometry — Hiroshi Nomura
5. Comparison of virulence factors, phylogenetic groups and ciprofloxacin susceptibility between *Escherichia coli* isolated from healthy students and uropathogenic *E. coli* isolated from patients with urinary tract infections in Korea — Min Park
6. The relationship between *Helicobacter pylori* infection and medical history of selected diseases among an urban area population of Japan — Akina Hayashi

– 10 minutes rest –

Session chair: Assistant Prof. Ki Jong Rhee

7. Anti-HCV agent ribavirin modulates transcription elongation in clotting factor VII expression — Atsuo Suzuki
8. Cervical condyloma acuminatum shows more progressive histopathological changes than vulvar condyloma acuminatum — Satomi Mizuno
9. Parkin induces apoptotic cell death in TNF-α-treated cervical cancer cells — Yoonjung Cho

– 5minutes rest –

Session chair: Prof. Takashi Murate

10. Parkin induces MMP-3 expression in human cervical cancer cells — Byung Chul Jung
11. Induction of the IL-2-independent growth by *KRAS* G12A mutation — Naoki Mizutani
12. Changes of matrix metalloproteinases (MMPs) expression in triglyceride treated macrophages. — Jaewon Lim

CANCER-DIRECTED DELIVERY OF DOXORUBICIN-RAPAMYCIN AND CANCER IMAGING BY ANTI-HER2 IMMUNOLIPOSOMES

Min Woo Kim, Yeon Kyung Lee, Hwa Yeon Jung, Seong Jae Kang, and Yong Serk Park

Department of Biomedical Laboratory Science, College of Health Science, Yonsei University, Wonju 220-710, Republic of Korea

Introduction

About 30% of human breast cancers overexpresses Her2/neu, implying clinically bad prognosis. Although doxorubicin, intercalating agent in the DNA double strand, has been known as an effective anticancer drug, Her2/neu-overexpressing cell lines such as SK-BR-3 have resistance to the drug via PI3K/AKT/mTOR signaling, associated with cell survival pathway. Therefore, we have tried to develop an effective treatment procedure for Her2-positive breast cancer by blocking of the PI3K/AKT/mTOR pathway. Rapamycin, acting as an immunosuppressant drug, is known to directly bind the mTOR Complex, so it appears to be an appropriate inhibitor to the PI3K/AKT/mTOR pathway. [2]

Combinational therapy with rapamycin and doxorubicin would presumably exhibit elevated anticancer efficacy to Her2-positive cancers. [3] One strategy to deliver the both drugs specifically to the cancer cells is to develop tumor-directed liposomal formulations. Doxorubicin was encapsulated into anti-Her2 immunoliposomes and rapamycin was incorporated in the lipid bilayers. Quantum dots, semiconductor nanocrystals having unique optical properties, were also incorporated in the system for cancer imaging.

Materials and Methods

Materials

POPC (1-palmitoyl-2-oleoyl-sn-glycero-3-phosphocholine), DSPE-PEG2000 (1,2-distearoyl-sn-glycero-3-phospho-ethanolamine-N-[methoxy(polyethylene glycol)2000]), DSPE-PEG2000-MAL (1,2-distearoyl-sn-glycero-3-phosphoethanolamine-N-[maleimide (polyethylene glycol)2000]) were purchased from Avanti Polar Lipid, Inc. (Alabaster, USA). PD-10 column and sepharose CL-4B was purchased from Amersham Bioscience (Uppsala, Sweden). Inorganic Quantum dots (dissolved in chloroform) were purchased from Nanosquare (Seoul, Korea).

Cell lines and cell culture

Her2/neu-positive SK-BR-3 (human breast cancer cell line) and Her2/neu-negative MDA-MB-231 (human breast cancer cell line) were maintained in DMEM (Gibco, Carlsbad, USA). The culture media were supplemented with 10% fetal bovine serum and 100 units/ml streptomycin.

Preperation of liposomes

PEGylated liposomes conjugated to Herceptin (Her2-targeted humanized antibody) were prepared according to the ethanol injection method. POPC, cholesterol, PEG-PE, PEG-maleimide and rapamycin were dissolved in 100 ul of ethanol at 60℃ (Table 1) and quantum dots were additionally added to the ethanol solvent. Then, the ethanol system was injected into 900 ul of degassed citrate buffer. (150 mM, pH 4.0) [1]

Table 1.Components of anti-Her2 immunoliposomes

lipid	mole%
POPC	48.00%
DSPE-PEG2000	3.80%
DSPE-PEG2000-Mal	0.20%
Cholesterol	48.00%

Direct coupling of thiolated anti-Her2 antibody to liposomes

Herceptin were thiolated for 1 hr at room temperature by reacting with Traut's reagent in degassed HEPES-EDTA buffer (20 mM HEPES, 140 nM NaCl, 2 mM EDTA, pH 8.0). Unreacted Traut's reagent was removed by passing through PD-10 column with the degassed HEPES buffer. Thiolated antibodies were added and then conjugated to the prepared liposomes by incubation for 16 hr at 4℃ with continuous agitation.

Doxorubicin encapsulation

Doxorubicin was encapsulated by the pH gradient method. [4] Briefly, the hydrated liposomes in a citrate buffer (150 mM, pH 4.0) were passed through the sepharose CL-4B column equilibrated with the HEPES buffer (20 mM HEPES, 140 nM NaCl, pH 7.5) to replace the extra-liposomal solution. Doxorubicin was added to the liposomal solution (1:3 weight ratio) and then incubated at 60℃ for 10 min with gentle mixing. The incubation process at 60℃ was necessary for rapid and complete entrapment of doxorubicin inside lipis vesicles.

Results

Preperation of anti-Her2 multifunctional immunoliposomes

A conceptual illustration of the anti-Her2 immunoliposomes is shown in Figure 1.

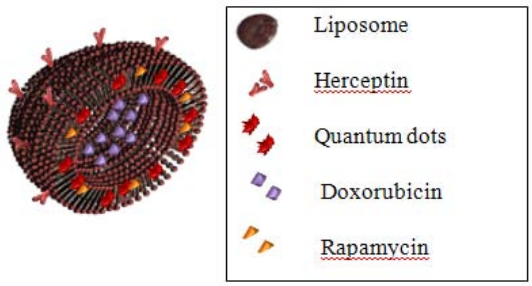

Figure 1. A diagram of Her2-targeted multifunctional immunoliposomes

After direct coupling of anti-Her2 antibodies, the liposomal solutions were passed through a sepharose CL-4B gel filtration column (Figure 2). The fraction 5-6 shows peak and represents liposome confirmed by the phosphate assay (650 nm) to detect lipid components, and by the Lowry protein assay (750 nm) to detect conjugated antibodies. Additionally, the fluorescence of Quantum dots was visualized by UV illumination.

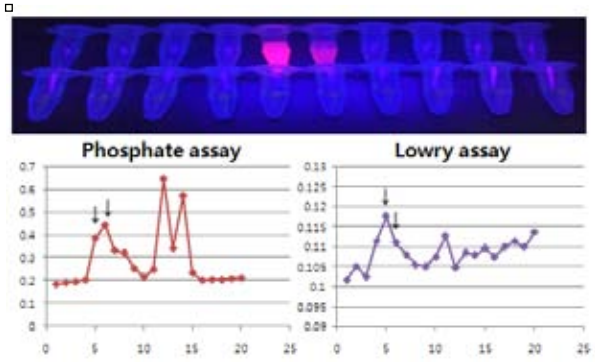

Figure 2. Elution profiles of anti-Her2 immunoliposomes.

Specific cellular binding of anti-Her2 immunoliposomes

Specific cellular binding of anti-Her2 multifunctional immunoliposomes was examined by FACS analysis and confocal microscopy. The anti-Her2 liposomes were able to specifically bind to Her2-positive SK-BR-3 cells, but not to Her2-negative MDA-MB-231 cells (Figure 3).

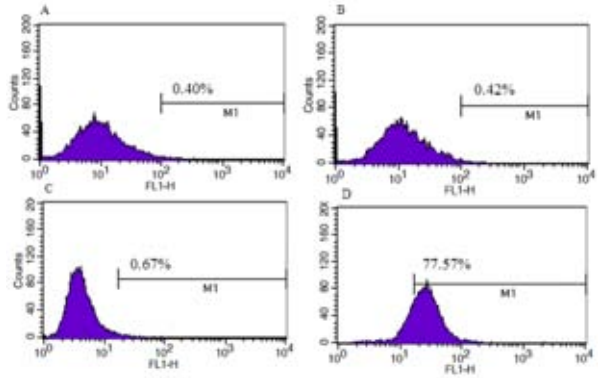

Figure 3. Binding of anti-Her2 multifunctional immunoliposomes to SK-BR-3 and MDA-MB-231 cancer cells.
A : MDA-MB-231, untreated
B : MDA-MB-231, treated with anti-Her2 immunoliposomes
C : SK-BR-3, untreated
D : SK-BR-3, treated with anti-Her2 immunoliposomes

Additionally, the anti-Her2 multifunctional immunoliposomes containing quantum dots were added to SK-BR-3 cells. After 3 hr incubation, red flurescences representing quantum dots were observed by confocal microsopy (Figure 4).

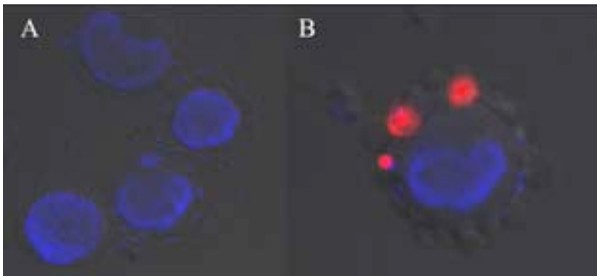

Figure 4. Binding of anti-Her2 multifunctional immunoliposomes containing qantum dots to SK-BR-3 cancer cells.
A : SK-BR-3, no treatment
B : SK-BR-3, anti-Her2 multifunctional immunoliposomes

Reference

[1] Muthu MS, Kulkarni SA, Raju A, Feng SS. Theranostic liposomes of TPGS coating for targeted co-delivery of docetaxel and quantum dots. Biomaterials. 2012 Apr;33(12):3494-501. Epub 2012 Feb 4

[2] Gnant M. The Role of Mammalian Target of Rapamycin (mTOR) Inhibition in the Treatment of Advanced Breast Cancer. Curr Oncol Rep. 2012 Sep 28.

[3] Wendel HG, De Stanchina E, Fridman JS, Malina A, Ray S, Kogan S, Cordon-Cardo C, Pelletier J, Lowe SW. Survival signalling by Akt and eIF4E in oncogenesis and cancer therapy. Nature. 2004 Mar 18;428(6980):332-7

[4] Nakamura K, Yoshino K, Yamashita K, Kasukawa H. Designing a novel in vitro drug-release-testing method for liposomes prepared by pH-gradient method. Int J Pharm. 2012 Jul 1;430(1-2):381-7. Epub 2012 Apr 12

Author address

E-Mail: nanodream@yonsei.ac.kr

Variation of IgE-binding epitopes in the allergen after repeated immunization

Takehiro Yamaguchi, Miyoko Matsushima, Nanako Ogasawara, Haruka Nose, Tsutomu Kawabe

Department of Pathophysiological Laboratory Sciences, Nagoya University Graduate School of Medicine, Nagoya, Japan

Introduction

The production of IgE antibodies to exposed allergen is needed to develop allergic responses. In humoral responses after primary exposure to allergen, naive B cells are differentiated into plasma cells but also differentiated into memory B cells. Plasma cells constitutively secrete antibody, which bind to the antigen. Memory B cells differentiate quickly into antibody secreting cells that are enhanced in production rate, titre and affinity from an original antibody when re-exposed to allergen [1, 2, 3]. However it is not clear whether memory B cells could continue to make antibody responses following repeated immunization of allergen.

Since the antibody produced by one B cell recognizes only one of the epitopes of the antigen that usually has multiple epitopes, several antibodies would be generated against the set of epitopes. We usually detect the quantity of allergen-specific IgE antibodies by the ELISA tests. The problems of the current ELISA test results in false positive and false negative with high frequency to diagnose allergen-specific allergic diseases because the current test detected only the conditions sensitized by allergen. Because the purified whole proteins were used as allergen to detect allergen-specific IgE antibody levels, we hypothesized that the information on the variations of epitopes recognized by IgE antibodies to cause allergic reactions might improve the accuracy to diagnose the allergy.

Recently the peptide microarray was used as versatile common tools for high throughput screening assay in biomedical and pharmaceutical research [4, 5]. Peptide arrays can evaluate the ligand–receptor interactions and epitope mapping. Using the peptide array, we can get more precise data on allergens detected by specific IgE antibodies. Therefore, the analysis of epitope patterns would identify the allergen-specific antibody to cause allergic reactions. Furthermore, this will lead us to understand the clinical tolerance of the allergy or the severity of the allergy symptom.

In this study, we examined the distribution pattern of allergen-specific IgE recognizing epitopes by using peptide array after repeated immunization of allergen.

Materials and Methods

Animals: 6 to 8 week-old female BALB/c mice were maintained in a temperature (22-24°C), humidity (55±5%), and light (12 hour light-dark cycle; lights on at 7:00) regulated room with food and water ad libitum. All procedures were performed with the approval of Medicine, Nagoya University in accordance with the Guidelines for Animal Experimentation of Nagoya University.

Immunization: Mice were sensitized i.p. in 0, 2, 4, 6, 10, 12, 16 and 20 weeks, with 100 μg of β-lactoglobulin together with 1 mg of alum in a final volume of 200 μl saline. Control mice were injected 200 μl saline containing 1 mg of alum. Before each immunization, mouse serum was collected.

Measurement of allergen-specific antibodies: β-lactoglobulin specific IgE levels were measured using ELISA. Microtitre plates were coated with β-lactoglobulin (25 μg/ well in 100 μl) overnight at 4 °C, and then blocked with 1% bovine serum albumin (BSA) for 1 h at room temperature (RT). The plates were washed with phosphate-buffered saline (PBS) with 0.05% Tween 20 (PBS-T). Serum samples were diluted 1 : 5 in 1% BSA, and incubated for 2 h at RT. Plates were then washed and incubated with biotin-labelled anti-mouse IgE antibodies for 2 h at RT. Followed by incubation with HRP-labelled streptavidin for 2 h at RT. Plates were developed using *o*-phenylenediamine substrate and optical density was measured at 490 nm using microplate reader.

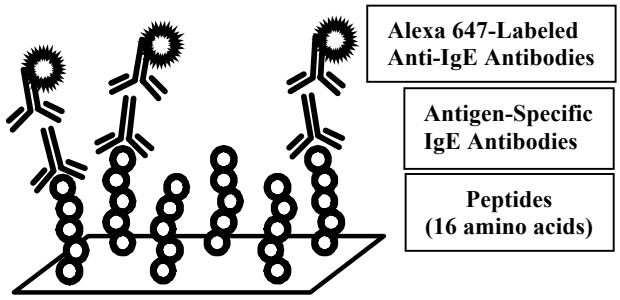

Fig1. IgE-binding analysis using the peptide array

IgE-binding analysis using the peptide array: A library of peptide used in this study consists of 16 amino acids overlapping by 13 (3-offset) and corresponds to the primary sequences of a β-lactoglobulin (UniprotKB P02754). Linear peptides were individually dissolved in a 20 mM phosphate buffer (pH 8.5) containing 0.1% sodium dodecyl sulfate (SDS). After the addition of 1-ethyl-3- (3-dimethylaminopropyl) carbodiimide hydrochloride (EDC), peptide solutions were spotted in at least triplicate on a succinimidyl-functionalized glass slide using the piezoelectric ceramic micropump (GENESHOT, NGKInsulators, Ltd., Aichi, Japan). Peptide array was blocked with blocking buffer containing 50 mM ethanolamine for 90 min. Then, the peptide array was washed 3 times for 5 min with PBS–T. Blood sera were diluted 1:10 in PBS-T containing 1% ovalbumin to a final volume of 200 μl. The diluted sera were then transferred to the surface of the slides and covered by a micro cover glass. The slides were incubated for 1 h at 37 °C, followed by overnight incubation at 4 °C. Then, the peptide array was washed 3 times for 5 min with PBS-T and incubated with Alexa 647-labeled anti-mouse IgE diluted 1:500 in PBS-T containing 1% ovalbumin for 3 h at RT in dark. The peptide arrays were finally washed 3 times in PBS-T and in distilled water for 5 min, and dried by centrifugation at 800 rpm for 3 min. All these steps were performed at room temperature. An Agilent microarray scanner (model G2505B, software G2565BA/DA; Agilent Technologies, Palo Alto, CA, USA) was used to analyse the fluorescence images of Alexa 647-labeled anti-mouse IgE at an emission wavelength of 665 nm. Fluorescence intensities were quantified with GenePix Pro (Axon, Union City, CA, USA).

Results

Detection of the β-lactoglobulin specific IgE

We first examined the allergen-specific IgE antibodies after immunization. Mice were immunized with β-lactoglobulin for 8 times. β-lactoglobulin-specific IgE were detected after primary immunization. High levels of β-lactoglobulin-specific IgE amount were maintained after subsequent immunization.

Variation of IgE-binding epitopes after repeated immunization

We next analysed the IgE-binding peptide patterns using mouse sera collected after each immunization (2, 6, 14, 18, and 22 weeks). β-lactoglobulin-specific IgE antibodies only bound to the set of peptides which include the peptide No. 20 and flanking peptides in 2 weeks after primary immunization. Furthermore, IgE bound to the similar pattern of peptides in 6 to 22 weeks after subsequent immunization. However, fluorescence intensities of these peptides was decreased in 6, 14, and 18 weeks but increased again in 22 weeks. We also detected the binding of IgE to the new set of peptides which include peptide No. 42 and flanking peptide in 14 weeks as 6th immunization proceeded. Similar pattern of epitopes was also observed in 18 and 22 weeks. In 18 weeks, the set of peptides which include peptide No.42 were detected the highest fluorescence intensities. Whereas, the set of peptides which include peptide No.33 were detected the highest fluorescence intensities in 22 weeks.

Discussion

In this study, we investigated the variations of IgE-binding epitopes after repeated immunization by using a peptide array.

First, we detected the epitopes bound by the mouse serum IgE using peptide array. The epitope recognized by an antibody was normally consisted of 7 to 8 amino acids, and we established a peptide array which was consisted of 16 amino acids overlapping by 13 (3-offset) and corresponds to the primary sequences of β-lactoglobulin. Therefore, we hypothesized that several fluorescence intensities were detected in flanking peptides which contains the epitope for each epitope that recognized by an antigen-specific IgE antibody. Thus, we thought fluorescence intensity detected in a single peptide was non-specific reaction to peptide that not contains an IgE-binding epitope.

Amazingly, we detected only one epitope recognized by β-lactoglobulin-specific IgE after primary immunization since several antibodies which recognize different epitopes was supposed to be generated against the β-lactoglobulin that has multiple epitopes. We also detected the similar pattern of epitope distribution by antigen-specific IgE antibodies in mouse serum, suggesting that memory B cells might be activated to produce β-lactoglobulin-specific IgE binding to same epitopes with repeated immunization. Furthermore, fluorescence intensities were decreased after consequent immunization, suggesting the activation of memory B cells was gradually declined in subsequent immunization. However, we could not exclude the possibility that the generation of these antibodies were from the activation of naïve B cells. We also detected the binding of IgE to the different set of epitopes as immunization proceeded. These results suggested that another newly activated B cells with the different epitopes recognized by β-lactoglobulin-specific IgE would be generated after second or subsequent immunization. Moreover, the degree of memory or naïve B cell activation might be different in every immunization since there was a shift of the peptide which has the highest fluorescence intensities in each serum. However, we could not detect the conformation-dependent epitopes recognized by β-lactoglobulin-specific IgE in our experimental conditions since antigen-specific IgE could bind only linear protein epitopes by peptide array.

Furthermore, the part of amino acid sequences of epitopes that we detected in this study were corresponded to the amino acid sequences that were important in cow`s milk allergy which previously reported [6].

To elucidate the role of memory B cells in repeated immunization, further studies should be done. Memory B cells are differentiated in germinal center through a process involving the acquisition of affinity maturation that enhance antigen binding [7]. Therefore, the measurement of affinity of antigen-specific IgE antibodies to each epitope would reveal whether memory B cell produces antibodies after repeated immunization.

Conclusions

In this study, we suggest that memory B cells seemed to be activated to produce antibodies in repeated immunization. However, there was a possibility that activation of memory B cells was not necessarily maintained in high levels after subsequent immunization. In parallel to the activation of memory B cells, allergen-specific IgE antibodies which recognize different epitopes would be newly generated.

References

[1] Benson, M.J., R. Elgueta, W. Schpero, M. Molloy, W. Zhang, E. Usherwood, and R.J. Noelle. Distinction of the memory B cell response to cognate antigen versus bystander inflammatory signals. *J. Exp. Med.* 2009; 206: 2013–2025.

[2] Dogan, I., B. Bertocci, V. Vilmont, F. Delbos, J. Mégret, S. Storck, C.A. Reynaud, and J.C. Weill. Multiple layers of B cell memory with different effector functions. *Nat. Immunol.* 2009; 10: 1292–1299.

[3] Pape, K.A., J.J. Taylor, R.W. Maul, P.J. Gearhart, and M.K. Jenkins. Different B cell populations mediate early and late memory during an endogenous immune response. *Science.* 2011; 331:1203–1207.

[4] Andresen H, Zarse K, Gro¨ tzinger C, Hollidt JM, Ehrentreich-Fo¨ rster E, Bier FF, et al. Development of peptide microarrays for epitope mapping of antibodies against the human TSH receptor. *J Immunol Methods*. 2006; 315:11–8.

[5] Nahtman T, Jernberg A, Mahdavifar S, Zerweck J, Schutkowski M, Maeurer Met al. Validation of peptide epitope microarray experiments and extraction of quality data. *J Immunol Methods.* 2007; 328:1–13.

[6] Kirsi-Marjut Järvinen, Pantipa Chatchatee, Ludmilla Bardina, Kirsten Beyer, and Hugh A. Sampson. IgE and IgG Binding Epitopes on α-Lactalbumin and β-Lactoglobulin in Cow's Milk Allergy. *Int Arch Allergy Immunol.* 2001; 126:111–118

[7] McHeyzer-Williams, L.J., and M.G. McHeyzer-Williams. Antigenspecific memory B cell development. *Annu Rev Immunol.* 2005; 23: 487–513.

Author address

E-Mail:yamaguchi.takehiro@c.mbox.nagoya-u.ac.jp

Evaluation of human papillomavirus oncogenic mRNA testing for diagnosis of cervical cancer by using real-time NASBA

Yeonim Choi1), Geehyuk Kim1), Sangjung Park1), Sunghyun Kim1), Yeon Kim1), Dongsup Lee2), Jijgee Munkhdelger3), Kwang Hwa Park3), and Hyeyoung Lee1)†

1)Department of Biomedical Laboratory Science, College of Health Sciences, Yonsei University, Wonju 220-701 Korea
2)Department of Clinical Laboratory Science, Hyejeon College, Hongseoung, Chungcheong Nam-do, Republic of Korea
3)Department of Pathology, College of Medicine, Yonsei University, Wonju 220-701, Korea

Introduction

Human cervical cancer is the third most common cancer among women worldwide [1]. In the past, cyto-pathological test, such as the Papanicolaou smear, was the only way of detecting invasive cervical carcinoma. Several decades ago, Human papillomaviruses (HPV) were found out to be a major factor of cervical cancer [2]. This finding was based on the observations that showed there is a significant association between oncogenic HPV infections and cyto-histologically defined pre-invasive lesions and invasive cervical carcinoma [3, 4]. Ever since then, the methods detecting HPV in clinical specimens became widely used for diagnosing cervical cancer.

Among those, DNA-based HPV genotyping assay has been the method of the choice, since it has shown high analytical sensitivity. However, the poor clinical specificity of the HPV genoytyping based on cervical cancer diagnosis has drawn serious clinical concerns. The latest results show oncogenic HPV DNA appeared not only in cancerous tissues, but also in the normal tissues according to cytological diagnosis.

Recently, a cervical diagnostic test employing real-time NASBA has been commercialized. The test detects E6 and E7 mRNA of oncogenic HPV, which are known to be responsible for oncogenesis of cervical cancer by HPV, instead of oncogenic HPV DNA. In this study, we evaluated the clinical sensitivity and specificity of the test for diagnosis of cervical cancer.

Materials and Methods

Cervical decidual cell samples were recruited at Yonsei University Wonju Christian Hospital in Gangwon province of Korea. A total of 187 cervical decidual cell samples were classified by 2001 Bethesda system (cyto-phathologic analysis) and were performed with HPV DNA genotyping test (DNA chip, Cancer Minichip kit, Goodgen).

For real-time NASBA test for diagnosis of cervical cancer, RNA was extracted using automation machine (MagNA Pure LC 2.0, Roche) and RNA Isolation High Performance Kit (Roche). The NASBA kit (NucliSENS EasyQ HPV, Biomerieux) used in this study targets E6 and E7 mRNA of HPV genotype 16, 18, 31, 33, 45. The NASABA was performed by the manufacturer's recommendation using the EASY Q NASBA ANALYSER (Biomerieux).

Results

A total of 138 samples were high-risk HPV positive by HPV DNA genotyping test and 49 samples were HPV DNA negative. Real-time NASBA test was performed with all of 187 samples. The positive rate of real-time NASBA test with high-risk HPV positive samples was 73.3% in SCC & ADC (squamous cell carcinoma & adenocarcinoma) group, 73.9% in HSIL (High-grade squamous intraepithelial lesion) group, 60% in ASC-H (Atypical squamous cells) group, 37.5 % in LSIL, 29.2% in ASC-US (Atypical squamous cells of undetermined significance) group, and 16.4% in normal group. On the other hand, the positive rate of real-time NASBA in normal group samples whose cytological findings were normal and HPV genotyping results were also negative samples was 0%.

Cytology results	DNA chip (goodgen kit)	Sample No. (U1A type positive)	Real-time NASBA (biomeriux) 16, 18, 31, 33, 45 type			qPCR
			Positive rate (%)	Negative rate (%)		
				*	**	GAPDH (ct)
SCC & ADC	High risk	15	11(73.3%)	3(20%)	1(6.7%)	25.3 ~ 28
HSIL	High risk	23	17(74%)	2(8.6%)	4(17.4%)	25.4 ~ 29.6
ASC-H	High risk	5	3(60%)	0(0%)	2(40%)	27.3 ~ 28.5
LSIL	High risk	16	6(37.5%)	6(37.5%)	4(25%)	23.7 ~ 29
ASC-US	High risk	24	7(29.2%)	14(58.3%)	3(12.5%)	21.9 ~ 28.1
Normal	High risk	55	9(16.4%)	35(63.6%)	11(20%)	20.1 ~ 28
Normal	Normal	49	0(0%)			
Total		187	53			

Conclusions

The data from this study seems clearly show that the real-time NASBA for diagnosis of cervical cancer has higher clinical specificity than HPV DNA genotyping test, since the positivity rate detected by the real-time NASBA in normal samples was significantly lower than that detected by the HPV DNA genotyping test. However, the positive rate detected by the real-time NASBA in cancerous samples was much lower than that detected by the HPV DNA genotyping test. In this respect, the sensitivity of the real-time NASBA for cervical cancer diagnosis seems to be lower than current

HPV genotyping test. This fact can be problematic in clinical settings. Therefore, the results from this study seem to suggest that for a real-time NASBA based cervical cancer test to be employed in clinical settings, more careful evaluations with large numbers of clinical specimens will be recommended.

References

[1] Jemal A, Bray F, Center MM, Ferlay J, et al. Global cancer statistics: GLOBOCAN 2008. *CA Cancer J Clin*. 2011;61:69–90

[2] F. Xavier Bosch, M. Michele Manos, Nubia Munoz, Mark Sherman, Angela M. Jansen, Julian Peto, Mark H. Schiffman, Victor Moreno, Robert Kurman, Keerti V. Shah. Prevalence of Human Papillomavirus in Cervical Cancer: a Worldwide Perspective. *Journal of the National Cancer Institute*. 1995;Vol. 87, No. 11, June 7.

[3] Walboomers JMM, Jacobs MV, Manos MM, Bosch FX, Kummer A, Shah KV, Snijders PJF. Human papillomavirus is a necessary cause of invasive cervical cancer worldwide. *J Pathol.* 1999;189:12–19.

[4] Bohmer G, van den Brule AJ, Brummer O, Meijer CL, Petry KU. No confirmed case of human papillomavirus DNA negative cervical intraepithelial neoplasia Grade 3 or invasive primary cancer of the uterine cervix among 511 patients. *Am J Obstet Gynecol.* 2003;189:118–120.

Author address
E-Mail : hyugiyoebi@naver.com
Corresponding author : hyelee@yonsei.ac.kr

Quantitation of neonicotinid metabolites in human urine using gas chromatography-mass spectrometry

H. Nomura[1)], J. Ueyama[1)], S. Wakusawa[1)], T. Kondo[1)]

1) Department of Pathophysiological Laboratory Sciences, Nagoya University Graduate School of Medicine, Nagoya, Japan

Introduction

Neonicotinoid insecticides (NEOs), developing as relatively new pesticides, act selectively on insect nicotinic acetylcholine receptors, and are widely used in agriculture as foliar and seed treatments, for indoor and outdoor insect control, home gardening and pet products (Jeschke et al., 2011). NEOs have from five to ten times higher selectivity factors for insects versus mammals than the organophopsphates, methylcarbamates, and organochlorines (Tomizawa and Casida, 2005). For this reason, NEOs are considered to be harmless to mammals and to be a promising candidate that could replace more toxic organophosphorus insecticides (OPs). NEO-induced toxicity in the nervous systems of vertebrates has been studied once in a while. It has been reported that such NEOs as thiamethoxam and clothianidin induce dopamine release in the rat striatum via nicotinic acetylcholine receptors (nAChRs) and that thiamethoxam alters behavioral and biochemical processes related to the rat cholinergic systems (Rodrigues et al., 2010). These findings suggest a possibility that NEOs affect mammalian nAChRs to a greater extent than previously believed based on general toxicity data obtained registration requirements tests for pesticide; this warrants further studies of the effect of NEOs on human health.

NEO metabolism has been addressed by Casida and colleagues. As shown in Fig. 1, NEOs such as imidacloprid, nitenpyram, thiacloprid and acetamiprid have a common structure chloropyridinyl, and these compounds metabolize into 6-chloronicotinic acid (6-CN), which is conjugated with glycine or glucuronic acid. Similarly, thiamethoxam and clothianidin have a common structure chlorothiazole, and both metabolize into 2-chloro-1,3-thiazole-5-carboxylic acid (2CTCA) also conjugated with glycine or glucuronic acid.

For the determination of urinary 6CN, high-performance gas chromatography tandem mass spectrometry (GC-MS/MS) combined with solid phase extraction (SPE) has been developed (Uroz et al., 2001). Their method showed a high-sensitivity performance (limit of detection 0.02 μg/L of urine), but required complicated sample procedures and GC-MS/MS is not affordable even now.

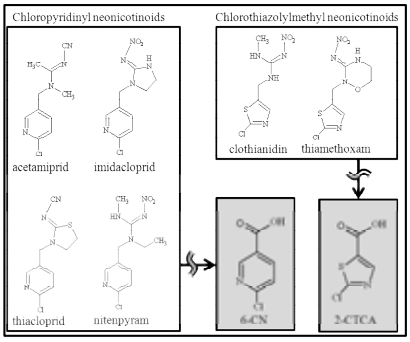

Fig. 1. Neonicotinoids and their urinary metabolites (shaded areas) measured for biological monitoring.

The main object of this study is to develop and validate a simple method for quantitation of urinary NEO metabolites, 6CN and 2CTCA, in human urine with GC-MS. The sensitivity and reliability of our method will be examined in this study.

Materials and Methods

Chemicals and reagents: 6CN (purity >98.0 %), hydrochloric acid (6 mol/L), formic acid, methanol were obtained from Wako Pure Chemicals (Osaka, Japan), and 2CTCA (purity > 98.0%) was from Santa Cruz Biotechnology, Inc (CA, USA). Isotope labeled 3-phenoxybenzoic acid (phenoxy-13C6, purity > 98%), for use as an internal standard (I.S.) substance, was purchased from Cambridge Isotope Laboratories, Inc (Ma, USA). N,O-bis(trimethylsilyl)trifluoroacetamide with 1% trimethylchlorosilane (BSTFA-TMCS, 99:1) and trimethylsilyldiazomethane were purchased from Tokyo Kasei Kogyo (Tokyo, Japan), acetonitrile and sulfuric acid were from Kanto Chemicals (Tokyo, Japan). 1,1,1, 3, 3, 3-Hexafluoroisopropanol (HFIP) and N,N-diisopropylcarbodiimide (DIC) were from Sigma-Aldrich (MO, USA). Polymeric strong cation exchange SPE products, the Bond Elute PCX (30 mg) (Agilent Technologies, Inc. CO, USA), was used for NEO metabolite extraction from urine.

Sample preparation procedure: Two milliliters of urine was pipetted into a 10-mL screw-top glass test tube, and 50 μL H_2SO_4 and I.S. solution (1 mg/L isotope labeled 3-PBA, d3PBA) were added. After gentle shaking, the test tube was incubated at 86 ^oC in a heat block for 2 hour for deconjugation. After cooling on ice, the test tube was centrifuged at 2,000×g for 10 min, and the supernatant was applied to SPE procedure.

A SPE cartridge packed into a 1-mL solvent reservoir was pre-conditioned with 500 μL methanol and followed by 500 μL water wash. Then, the conditioned SPE was loaded with 2 mL urine sample and placed under a vacuum pressure and followed by 500 μL formic acid solution (2%) wash. The SPE cartridge was dried under vacuum for 3 min and eluted with 500 μL methanol. The eluate was dried up with a gentle nitrogen stream at room temperature and the residue was resolved with 500 μL acetonitrile. Thirty minutes after the addition of 50 μL derivatization reagent, BSTFA-TMCS, 1 μL sample was analyzed by GC-MS within 24 hours after the derivatization.

Results and discussion

Derivatization condition: First of all, to perform highly sensitive determination, the optimum derivatization reagents and relevant conditions including reaction solution and temperature were examined. Previously, Uroz and colleagues (2001) derivatized 6CN with HFIP and DIC in hexane solution at room temperature for GC-based analysis. In our results as shown in Table 1, higher total ion chromatograph peak areas of 2CTCA and 6CN were detected when BSTFA-TMCS in either solution of acetonitrile or toluene was used for derivatization than with other conditions. Increase of reaction temperature

Table 1. Relationship between derivatization reagents and reaction efficiency in various solutions at room temperature for 30 min

(peak area, million)	acetonitrile	methanol	ether	toluene
2CTCA[a]				
HFIP[c]	3.5	-	3.1	4.2
BSTFA-TMCS[d]	4.3	-	1.9	4.5
Trimethylsilyldiazomethane	2.4	2.6	1.0	0.7
6CN[b]				
HFIP	3.2	-	3.1	3.3
BSTFA-TMCS	4.2	-	1.7	4.2
Trimethylsilyldiazomethane	1.8	2.4	1.1	1.3

Reaction efficiency is represented by the peak area obtained under various derivatization conditions.
[a]2CTCA, 2-chloro-1,3-thiazole-5-carboxylic acid.
[b]6CA, 6-chloronicotinic acid.
[c]HFIP, 1,1,1, 3, 3, 3-Hexafluoroisopropanol.
[d]BSTFA-TMCS, N,O-Bis(trimethylsilyl)trifluoroacetamide with 1% trimethylchlorosilane.

from room temperature to 60°C did not affect the peak areas dramatically. Toluene is considered to be an inconvenient solution for derivatization procedure due to its relatively high volatility and flammability. Our result indicates that use of BSTFA-TMCS in acetonitrile is the most efficient for derivatization at room temperature for 30 min to determine urinary NEO metabolites. We selected this optimum derivatization conditions in the later fundamental examination and applications. The full-scan mass spectora of trimethylsilyl-2CTCA and trimethylsilyl-6CN were shown in Fig. 2.

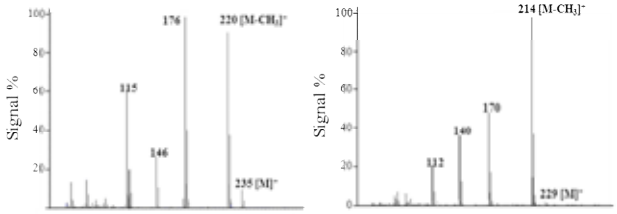

Fig. 2. Mass spectrum of derivatized 2CTCA (left) and 6CN (light).

Fig. 3 shows selected ion chromatograms of pooled urine samples spiked with 2CTCA (upper, m/z 220) and 6CN (lower, m/z 214). Our method yielded highly resolved peaks, allowing clear identification of NEO metabolites even at low concentration levels. No apparent interference peaks were observed. The most abundant ion derived from 2CTCA was the fragmentation ion at m/z 176 but its peak was interfered by an unknown peak. Thus, we selected the second largest fragment ion at m/z 220 as Q-ion.

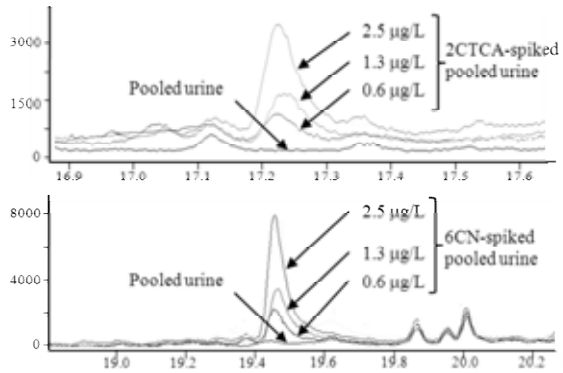

Fig. 3. GC-MS selected ion monitoring chromatogram of 2CTCA (top) and 6CN (bottom) in standard spiked pooled urine samples.

Accuracy, precision and linearity: The accuracy, precision and linearity parameters are summarized in Table 3. The regression equations were y=0.0054x+0.0002 (r^2=0.999) for 2CTCA and y=0.013x+0.0015 (r^2=0.999) for 6CN. The

Table 2. Accuracy, precision, LOD and LOQ data of analytical procedure.

	Pooled urine spiked concentration (µg/L urine)	n^a	2CTCA	6CA
Within-run				
Precision (%RSD[b])	0.6	5	5.4	5.2
	1.3	4	7.6	8.2
	2.5	5	8.5	3.7
	5	5	5.5	9.5
	10	5	6.2	7.4
Mean recovery[c]	0.6	4	103	101
	5	5	88	93
R^2 of calibration line			0.999	0.999
LOD[d] (µg/l) (signal-to-noise ratio = 3)			0.1	0.1
LOQ[e] (µg/l) (signal-to-noise ratio = 10)			0.3	0.3

[a] *n*: number of observations.
[b] RSD: relative standard deviation.
[c] Recovery given by adding the standards just before derivatization step.
[d] LOD: limit of detection.
[e] LOQ: limit of quantitation.

LOD and LOQ were calculated to be 0.1 and 0.3 µg/L for both metabolites, respectively. The LOD value of 6CN was about six times higher than previously reported ones using GC-MS/MS (Uroz et al., 2001). Taira and colleagues reported a 6CN determination method with the LOQ of 1 µg/L using LC-MS. Although the LOD levels of our method are not as low as those in the previous reports, some advantages of our method was confirmed; i.e., simple sample preparation and use of commonly-used apparatus that provide stable assay results. We believe that this method might be useful for high-throughput analyses. Besides, no method of determining 2CTCA in urine has been previously reported to our knowledge. Our results indicate that the assay had remarkable reproducibility with acceptable accuracy and precision.

Application of the method to field study samples: Our method was applied for human spot urine obtained from nine apple farmers collected in August 2009. Based on their questionnaire response, four farmers who worked for NEO handling operation within 10 days before urine collection were selected as the occupational NEO exposure group. Mean concentrations of 6CN (above LOD) were 1.7 µg/L for the occupational exposure group and 1.3 µg/L for the control group. A 2CTCA concentration of 0.1 µg/L was detected only in one person in the exposure group. To our knowledge, this is the first report about the determination method of urinary 2CTCA and detection of 2CTCA from human urine.

In conclusion, a simple, sensitive and reliable method of GC-MS with SPE sample preparation for the determination of urinary 2CTCA and 6CN was developed. Since urinary 2CTCA and 6CN can be measured simultaneously, our method is expected to practically serve for the biomonitoring of NEO exposure at the individual level.

References

P. Jeschke, R. Nauen, M, Schindler, A. Elbert, J Agric. Food Chem. 59 (2011) 2897.

M. Tomizawa and J.E. Casida. Annu. Rev. Pharmacol. Toxicol. 45 (2005) 247

K.J. Rodrigues, M.B. Santana, J.L. Do Nascimento, D.L. Picanco-Diniz, L.A. Maues, S.N. Santos, V.M. Ferreira, M. Alfonso, R. Durán, L.R. Faro. Ecotoxicol. Environ. Saf. 73 (2010) 101.

F.J. Uroz, F.J. Arrebola, F.J. Egea-González, J.L. Martínez-Vidal. Analyst. 126 (2001) 1355.

Author address
E-Mail: nomura.hiroshi@h.mbox.nagoya-u.ac.jp

Comparison of virulence factors, phylogenetic groups and ciprofloxacin susceptibility between *Escherichia coli* isolated from healthy students and uropathogenic *E. coli* isolated from patients with urinary tract infections in Korea

M. Park[1)], S. Park[1)], S-H. Kim[1)], G. Lee[1)], H. Woo[1)], Y. Uh[2)], W-D. Seo[3)] and J. Kim[1)]

1) Department of Biomedical Laboratory Science, College of Health Science, Yonsei University, Wonju, Korea
2) Department of Laboratory Medicine, Yonsei University Wonju College of Medicine, Wonju, Korea
3) Department of Functional Crop, NICS, Miryang, Korea

Introduction

Uropathogenic *Escherichia coli* (UPEC) is one of the most common etiological agents in urinary tract infections. UTIs consist of such as asymptomatic bacteriuria, acute cystitis and acute pyelonephritis, etc. [1][2]. Causative agent of urinary tract infections include *E. coli*, *Proteus* spp., *Enterobacter aerogenes*, *Pseudomonas aeruginosa*, *Enterococcus faecalis*, *Staphylococcus aureus*, *Staphylococcus saprophyticus* and *Klebsiella pneumonia* [3][4]. UPEC cause urinary tract infections with the rate for 70-90% of community-acquired UTIs and approximately 40% of all nosocomial UTIs in the Unite States [5].

UPEC strains generally possess several genes encoding virulence factors, which are mostly adhesions, toxins, bacteriocin and siderophores [6]. Pathogenic *E. coli* strains, including UPEC strains, belong mainly to groups B2 and D [7]. Fluoroquinolones are commonly used for UTIs treatment in Korea, and resistance to fluoroquinolones is increasing, especially resistance to ciprofloxacin. In the current study, comparison of virulence factors (P and S fimbriae, type 1 fimbriae, α -hemolysin, uropathogen-specific protein and cytotoxic necrotizing factor 1), phylogenetic groups (A, B1, B2 and D) and ciprofloxacin susceptibility were examined between *E. coli* isolated from healthy students and uropathogenic *E. coli* isolated from patients with urinary tract infections in Korea..

Materials and Methods

Specimen collection

- A total of 188 strains of 175 UPEC clinical isolates was collected from Korean healthcare facility in 2010 and 13 strains were collected from healthy students in 2011.

Bacterial DNA extraction

- To prepare DNA templates, brain heart infusion (Difco, Detroit, USA) broth was inoculated with one colony of UPEC strain. After 18 hours incubation at 37°C, 1 ml of the culture were centrifuged at 12,000g for 10 minutes. The pellets were resuspended in 1 ml of saline, harvested by centrifugation and suspended in 200 μl of sterile water, incubated at 100°C for 10 min, and centrifuged. The supernatant was used in all PCRs as described below.

PCR (Polymerase Chain Reaction) amplification

- Determination of phylogenetic group was performed by a triplex PCR method was performed, which identifies type A, B1, B2 and D [7].
- Determination of genetic virulence profiles by multiplex PCR method, which detect fragments of genes encoding selected *E. coli* VFs (*hly*1, *fim*G/H, *usp*, *cnf*1, *pap*C, and *sfa*D/E) [6]

Ciprofloxacin susceptilibity test

- Each strains was screened for susceptibility (by the disk diffusion method) to ciprofloxacin

Results

The identified virulence factors (VFs), phylogenetic groups and cipofloxacin resistance in 13 *E. coli* strains isolated from healthy students were *pap*C (15.4%), *fim*G/H (76.9%), *sfa*D/E (30.8%), *hly*A (23.1%), *cnf*1 (23.1%), *usp* (7.7%), phylogenetic group A (23%), B1 (8%), B2 (46%), D (23%) and ciprofloxacin resistance (7.7%) , while those of in 175 *E. coli* strains isolated from patients with UTI were *pap*C (41.1%), *fim*G/H (92.5%), *sfa*D/E (30.3%), *hly*A (10.3%), *cnf*1 (30.3%), *usp* (27.4%), phylogenetic group A (9.1%), B1 (5.1%), B2 (60.6%), D (25.1%) and ciprofloxacin resistance (29.7%).

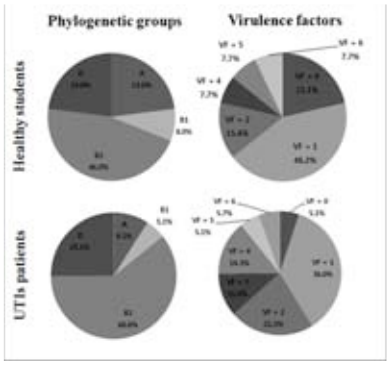

Figure 1. Distribution of phylogenetic groups and virulence profiles of *E. coli* strains isolated from healthy students and UTIs patients.

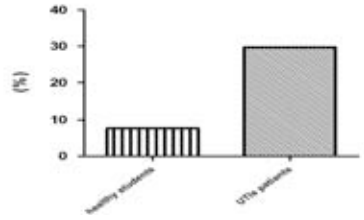

Figure 2. Distribution of resistance to ciprofloxacin of *E. coli* strains isolated from healthy students and UTIs patients. Ciprofloxacin resistance was found in strains from healthy students (7.7%) and UTIs patients (29.7%).

Conclusions

In our study, *E. coli* strains (76.9%) from healthy students were found to possess more than one virulence factor associated with adhesion. In addition, one *E. coli* strain isolated from healthy students who had never been infected with UPEC showed ciprofloxacin resistance (7.7%). Furthermore, UPEC strains isolated from patients showed high level of ciprofloxacin resistance. Because resistance to ciprofloxacin has approached 30%, ciprofloxacin should be considered as a first-line empirical treatment for UTIs after the proper antimicrobial susceptibility test.

References

[1]Fhin SD. Clinical practice. Acute uncomplicated urinary tract infection in Women. *N Engl J Med*. 2003. 17;349(3):259-266.

[2]Lee WY, Kim JB. Serological studies on the specific antibodies against p-pili of uropathogenic *Escherichia coli*. *Korean J Biomed Lab Sci*. 1996. 2(1):31-40

[3]DeBoy JM, Wachsmuth IK, Davis BR. Hemolytic activity in enterotoxigenic and non-enterotoxigenic strains of *Escherichia coli*. *J Clin Microbiol*. 1988. 12(2):193-198.

[4]Gupta K, Hooton TM, Stamm WE. Increasing antimicrobial resistance and the management of uncomplicated community acquired urinary tract infections. *Ann Intern Med*. 2001. 135(1):41-50.

[5]Li D, Liu B, Guo D, Guo X, Liu F, Feng L, Wang L. A multiplex PCR method to detect 14 *Escherichia coli* serogroups assocated with urinary tract infections. *J Microbiol Methods*. 2010. 82(1);71-77.

[6]Adamus-Bialek W, Wojtasik A, Majchrzak M, Sosnowski M, Parniewski P. (CGG)4-Based PCR as a Novel Tool for Discrimination of Uropathogenic *Escherichia coli* strains: Comparison with Enterobacterial Repetitive Intergenic Consensus-PCR. *J Clin Microbiol*. 2009. 47(12);3937-3944.

[7]Clermont O, Bonacorsi S, Bingen E, Rapid and simple determination of the *Escherichia coli* phylogenetic group. *Appl Environ Microbiol*. 2000. 66(10);4555-4558.

Author address

E-Mail: pm1984@naver.com

The Relationship Between *Helicobacter Pylori* Infection and Medical History of Selected Diseases among an Urban Area Population of Japan

A. Hayashi[1)], T. Kondo[1)]

1) Department of Pathophysiological Laboratory Sciences
Nagoya University Graduate School of Medicine, Nagoya, Japan

Introduction

Since successfully isolated and cultivated by Robin Warren and Barry Marshall in 1983, *Helicobacter pylori* (*H. pylori*) has become a high-profile organism. *H. pylori* is a helix-shaped, microaerophilic Gram-negative bacterium. In the infected stomach where normal secretion of urea usually occurs, large amounts of urease produced by *H. pylori* breaks down urea into ammonium to neutralize gastric acid, which helps *H. pylori* survive the acidic pH of the gastric lumen.

There has been established evidence indicating a strong association of *H. pylori* infection with the development of chronic active gastritis and peptic disease of the stomach and duodenum. Also, evidence showing long-standing infection to be an essential risk factor for gastric cancer is growing, while mechanisms by which *H. pylori* increases the risk of cancer have been vigorously investigated. In addition, involvement of *H. pylori* infection in the pathogenesis of extragastric disorders such as chronic urticaria, iron deficiency anemia, and idiopathic thrombocytopenic purpura has also been suggested.

H. pylori is so ubiquitous that over half of the world's population are considered to harbor the organism, with high prevalence in developing countries and decreasing incidence in industrialized countries. Unlike Western nations, however, Japan has an exceptionally high *H. pylori* infection rate of presumably as high as 50% of the population, though the rate is on the steady decline. Though the exact route of transmission is still unknown, the contagion is most likely to occur via either the oral-to-oral or fecal-to-oral contact. This contact includes mouth-to-mouth feeding from infected mothers to children at weaning ages and intake of fecally-polluted water or food. In the unsanitary environment, supply of drinking water from wells, streams, or ponds, and sanitary insects or animal waste can also be the source of infection.

A large body of literature has linked *H. pylori* infection to chronic gastritis, peptic ulcer, and gastric cancer; these associations were mostly studied in clinical or case-control research design, however. In Japan, prevalence of *H. pylori* infection in general populations has been previously studied in rural areas, but no such studies were performed in urban areas, with the exception of a study that we conducted in the Metropolitan City of Nagoya. The purpose of this study is to examine the association between *H, pylori* infection with medical history of various gastrointestinal and liver diseases.

Materials and Methods

In 2005, a long-term cancer cohort study, the Japan Multi-Institutional Collaborative Cohort Study (J-MICC Study), was launched, which mainly focuses on gene-environment interactions for cancer incidence. As one of 12 affiliated institutions, the Nagoya University Graduate School of Medicine team enrolled 5,167 voluntary residents (1,467 males and 3,700 females) aged 35 to 69 years old between June of 2008 and May of 2010. The enrolment took place at the Daiko Medical Center of Nagoya University (Daiko Study), and all the participants gave written informed consent.

The participants provided urine samples for the detection of anti-*H. pylori* antibody by using the commercially available antibody kit Rapiran (Otsuka Pharmaceutical Co. Ltd,. Tokyo, Japan). Positive test results were defined as presence of persistent *H. pylori* infection, and negative results as absence in this study. The questionnaire in this study covered various aspects of health-related lifestyles such as smoking and drinking history, dietary habit, and physical activity. Also included in the questionnaire was a history of *H. pylori* test and eradication treatments with or without successful results. History of past and present illness was also elicited by the questionnaire. For statistical analyses, we selected seven self-reported diseases of stomach ulcer, duodenal ulcer, chronic gastritis, diabetes, colon polyp, hepatitis B, and hepatitis C, which were regarded as outcome events. To model the association between these events and persistent *H. pylori* infection, multivariate-adjusted odds ratios were estimated using the logistic regression method. We conducted statistical analyses by running a free software R on Windows 7. The study protocol was approved by the ethics committee of the Nagoya University School of Medicine.

Results

After exclusion of those with successful previous eradication and unknown treatment results, a total of 4,753 (1,283 males and 3,470 females) subjects were available for the current analyses. Profiles of the subjects were presented in Table 1.

Table 1. Characteristics of the study population

	Male (n=1,283)	Female (n=3,470)
Age (years)		
35-39	175	553
40-44	146	462
45-49	166	510
50-54	174	446
55-59	180	437
60-64	207	526
65-69	235	536
average±SD	53.2±10.3	52.0±10.3
Results of test for *H. pylori*		
negative	779	2,246
positive	504	1,224

The overall *H. pylori* infection rate of 36.4% (39.2% for males and 35.3% for females) seems to be lower than expected, considering the relatively high mean age of our study population.

For both sexes, the logistic regression analysis revealed a statistically significant association between a history of peptic disease and *H. pylori* infection as determined by the

presence of anti-*H. pylori* antibodies; i.e., the risk for stomach/duodenal ulcer seems to be elevated in association with *H. pylori* infection (Table 2). History of chronic gastritis was also predicted by the persistent infection in both male and female subjects. A significant negative association was demonstrated between *H. pylori* infection and diabetes history in males, while no such significant association was observed in females. History of colon polyp, hepatitis B, and hepatitis C failed to show any significant relationships with persistent *H. pylori* infection in both sexes.

Table 2. Odds ratio (OR) and 95% confidence interval (95% CI) for the association between *H. pylori* infection and medical history of selected diseases

	Male		Female	
	OR	95% CI	OR	95% CI
Stomach ulcer	1.43	1.03–1.97	1.29	1.00–1.66
Duodenal ulcer	1.75	1.20–2.55	1.54	1.10–2.17
Peptic ulcer	1.67	1.25–2.22	1.30	1.04–1.63
Chronic gastritis	1.36	0.95–1.95	1.36	1.09–1.69
Diabetes	0.56	0.31–0.84	1.29	0.82–2.04
Colon polyp	0.93	0.65–1.33	0.84	0.59–1.19
Hepatitis B	1.26	0.52–3.02	0.60	0.29–1.15
Hepatitis C	2.86	0.75–1.38	0.97	0.35–2.55

Discussion

In consistent with previous findings, our results indicated a strong association between *H. pylori* infection and peptic ulcers of the stomach and duodenum. However, the observed inverse association between the infection and diabetes among male subjects remains to be explored. We hypothesized that among our male subjects, who seem to be prone to peptic disease as compared with females, capability of sugar absorption in their intestine might be affected, resulting in a lowered risk for the development of diabetes.

Conclusions

The current study demonstrated that residents in urban areas of Japan are less likely to harbor *H. pylori* than those in other areas. While the association between *H. pylori* infection and such diseases as peptic ulcer and chronic gastritis were found consistent with that from previous reports, it remains an open question whether *H. pylori* infection provides protection against type 2 diabetes.

References

[1] Marshall BJ, Warren JR. Unidentified curved bacilli on gastric epithelium in active chronic gastritis. *Lancet* 1983; 1:1273-75.

[2] Hamajima N, Goto Y, Nishio K, Tanaka D, Kawai S, Sakakibara H, Kondo T. *Helicobacter Pylori* eradication as a preventive tool against gastric cancer. *Asian Pac J Cancer Prev* 2004;5:246-52.

[3] Hamajima N, Naito M, Kondo T, Goto Y. Genetic factors involved in the development of *Helicobacter pylori*-related gastric cancer. *Cancer Sci* 2006;97:1129-38.

[4] Morita E, Hamajima N, Hishida A, Aoyama K, Okada R, Kawai S, Tomita K, Kuriki S, Tamura T, Naito M, Kondo T, Ueyama J, Kimata A, Yamamoto K, Hori Y, Hoshino J, Hamamoto R, Tsukamoto S, Onishi J, Hagikura S, Naito H, Hibi S, Ito Y, Wakai K. Study profile on baseline survey of Daiko Study in the Japan Multi-Institutional Collaborative Cohort Study (J-MICC Study). *Nagoya J Med Sci* 2011;73:187-95.

[5] Tamura T, Morita E, Kondo T, Ueyama J, Tanaka T, Kida Y, Hori Y, Inoue S, Tomita K, Okada R, Kawai S, Hishida A, Naito M, Wakai K, Hamajima N. Prevalence of *Helicobacter Pylori* infection measured with urinary antibody in an urban area of Japan, 2008-2010. *Nagoya J Med Sci* 2012;74:63-70.

Author address

E-Mail: hayashi.akina@f.mbox.nagoya-u.ac.jp

Anti-HCV agent ribavirin modulates transcription elongation in clotting factor VII expression

Atsuo Suzuki[1, 2)], Eriko Okuyama[1)], Moe Murata[1)], Yumi Ando[1)], Yuki Takagi[1)], Io Kato[1)], Akira Takagi[1)], Takashi Murate[1)], and Tetsuhito Kojima[1)]

1) Department of Pathophysiological Laboratory Sciences, Nagoya University Graduate School of Medicine
2) Japan Society for the Promotion of Science Research Fellow

Introduction

Factor VII (FVII), a vitamin K-dependent plasma glycoprotein, is synthesized in the liver and secreted into the blood. Once vascular injury occurrs, FVII forms a complex with tissue factor, and works as a trigger for blood coagulation.

In 2006, Yamamoto et al. reported that the anti-hepatitis C virus (HCV) agent ribavirin elevated the activity of FVII, leading to reduced doses of clotting factors used in hemostatic therapy for haemopillia patients with chronic hepatitis C [1]. They also demonstrated increased mRNA expression of the FVII gene (*F7*) by ribavirin treatment in human hepatoma cell lines (HepG2) and in cultured human hepatocytes; however, the detailed molecular mechanisms for this phenomenon remains unknown.

Ribavirin is a purine nucleoside analog used in anti-HCV therapy. The candidate mechanisms for the anti-viral actions of ribavirin include inhibition of RNA-dependent RNA polymerase activity in HCV or of the activity of inosine-monophosphate dehydrogenase (IMPDH) to decrease the intracellular GTP pool, and modulating the immune system [2]. Although the actions of ribavirin are partially understood, the mechanisms are not completely clear.

The aim of our study was to further investigate the molecular mechanisms underlying increased FVII mRNA expression by ribavirin treatment in HepG2 cells. It is important to elucidate the molecular basis of ribavirin before understanding its *in vivo* functions.

Materials and Methods

Cell culture and quantitative RT-PCR– The human hepatoma cell line (HepG2) was purchased from the American Type Culture Collection (ATCC, Manassas, VA, USA) and cultured as described previously [3]. Total RNA was extracted from the cells using the RNeasy mini kit (QIAGEN, GmbH, Germany) and the first strand cDNA was prepared from 1 μg of total RNA using the PrimeScript RT reagent kit (TaKaRa, Kyoto, Japan). Quantitative RT-PCR was performed with SYBR Premix ExTaq II (TaKaRa). Relative mRNA expression levels were calculated as the respective mRNA/GusB mRNA.

Nuclear run-on assay and nascent RNA capturing– The nuclear run-on assay was performed as reported previously with minor modifications [4]. Newly synthesized RNA transcripts were determined by the Click-iT Nascent RNA Capture Kit (Invitrogen) according to the manufacturer's protocol. HepG2 cells were cultured with or without ribavirin (100 μg/mL) for 16 h and subsequently pulsed with 0.2 mM 5-ethynyl uridine (EU) at 37 °C for 8 h. The cells were washed and collected, and total RNA was extracted. Click reaction was performed using 5 μg of EU-labeled RNA and 0.5 mM biotin azide; the mixture was incubated at room temperature for 30 min. Following RNA precipitation, the RNA was dissolved in 50 μL of RNase-free water. Biotin-labeled EU-RNA-binding pull-down assay was performed using 50 μL of Dynabeads MyOne Streptavidin and the bound RNA was washed and used as a template for reverse transcription. The captured nascent RNA was analyzed using qRT-PCR as described above.

RNA interference– HepG2 cells were transfected with ELL3-specific siRNA (siGENOME SMARTpool siRNA, Human ELL3; Dharmacon, Lafayette, CO, USA) or nonspecific siRNA (siGENOME Non-Targeting siRNA#3; Dharmacon) using Lipofectamine RNAiMAX (Invitrogen) by the reverse transfection protocol according to the manufacturer's protocol.

Chromatin immunoprecipitation (ChIP)– ChIP assay was performed as described previously with minor modifications [3]. The chromatin supernatants were immunoprecipitated with respective antibodies specific to Pol II 4H8, Pol II CTD pSer2, Pol II CTD pSer5 (Abcam), CDK9, AFF4, ELL3, and nonspecific normal rabbit IgG (Santa Cruz Biotechnology) at 4 °C for 3 h. The protein–antibody complexes were incubated with Dynabeads Protein G at 4 °C for 1 h. Bound DNA was purified used as a template for subsequent quantitative PCR.

Results and Discussion

We observed that ribavirin treatment increased FVII mRNA expression in HepG2 cells in a dose- and time-dependent manner. Ribavirin is a purine nucleoside analog, which could be incorporated into hepatocytes via equilibrative nucleoside transporter (ENT) [5]. We treated HepG2 cells with ENT inhibitor NBMPR together with ribavirin, and observed NBMPR completely abolished ribavirin-induced FVII upregulation.

Incorporated ribavirin is metabolited to ribavirin monophosphate (RMP) or ribavirin triphosphate (RTP). RMP is known as a inhibitor of IMPDH, which is a rate-limiting enzyme in a purine metabolism. It is known that inhibition of IMPDH causes intracellular GTP depletion, and that the GTP reduction could be reversed by supplementation with guanosine in a salvage pathway [6]. Then, we tested other IMPDH inhibitors, mycophenolic acid (MPA) and 6-mercaptopurine (6-MP), and found that they also induced FVII upregulation in HepG2 cells. The upregulation was canceled by addition of guanosine. Although we could not clarified why intracellular GTP reduction caused FVII gene upregulation, there may be a close relationship between GTP depletion caused by sequential inhibition of IMPDH and FVII upregulation.

Next, we investigated how FVII transcription was modulated by ribavirn treatment in HepG2 cells. In general, control of gene expression in eukaryotic cells involves regulatory events at multiple transcriptional and post-transcriptional stages. Transcription by RNA polymerase II (Pol II) is divided into four stages: initiation, promoter clearance, elongation, and termination. We analyzed which step of transcription was critical for ribavirin-induced FVII mRNA upregulation. First, we found that ribavirin treatment did not affect the FVII mRNA stability. Second, we performed luciferase-reporter analyses,

which reflects promoter initiation and clearance, to determine the *F7* promoter activity, but could not observed enough activation by ribavirin. In contrast, ribavirin treatment sufficiently increased nascent FVII mRNA synthesis in HepG2 cells, as analyzed by the nuclear run-on and nascent mRNA capturing assay, which reflects activation of transcription elongation. The *F7* upregulation was abolished by inhibiting CDK9 by DRB. CDK9 is a component of positive-transcription elongation factor b (P-TEFb), and P-TEFb is a major transcription factor which contributes the transcription elongation event [7, 8]. These findings demonstrated that ribavirin-induced *F7* upregulation is mainly induced by acceleration of transcription elongation associated with P-TEFb.

Further chromatin immunoprecipitation (ChIP) assays revealed that recruitment of Pol II and CDK9, and phosphorylation of Ser2 (pSer2) of the Pol II C-terminal domain (CTD) were reinforced by ribavirin treatment. The levels of pSer2 of CTD could be a marker of enhanced transcription elongation phase [7, 8]. To further investigate the other molecules which were necessary for increased FVII mRNA expression, we searched "ribavirin-responsive genes" by cDNA microarray analysis. We found that transcription elongation factor ELL3 expression was significantly upregulated in HepG2 cells treated with ribavirin, and that the ELL3 upregulation was induced in response to intracellular GTP depletion. In addition, we found ribavirin induced an increase in ELL3 mRNA expression before an increase in FVII mRNA expression in HepG2 cells, and ELL3 was recruited to the *F7* by ribavirin treatment. Knockdown of ELL3 by RNAi resulted in diminished FVII upregulation. These results suggested that transcription elongation factor ELL3 contributed ribavirin-induced FVII upregulation in HepG2 cells.

Taken together, in this study we found that ribavirin increased FVII mRNA expression by acceleration of its transcription elongation in HepG2 cells. The enhanced transcription elongation was induced by CDK9 kinase activity of P-TEFb and associated with ELL3. Although further study is required to determine why intracellular GTP depletion causes accelerated *F7* transcription elongation, our findings have contributed to elucidate the precise mechanisms of ribavirin-induced *F7* upregulation.

References

[1] Yamamoto, K., Honda, T., Matsushita, T., Kojima, T. and Takamatsu, J. (2006) Anti-HCV agent, ribavirin, elevates the activity of clotting factor VII in patients with hemophilia: a possible mechanism of decreased events of bleeding in patients with hemophilia by ribavirin. J. Thromb. Haemost. **4**, 469-470

[2] Feld, J. J. and Hoofnagle, J. H. (2005) Mechanism of action of interferon and ribavirin in treatment of hepatitis C. Nature **436**, 967-972

[3] Suzuki, A., Sanda, N., Miyawaki, Y., Fujimori, Y., Yamada, T., Takagi, A., Murate, T., Saito, H. and Kojima, T. (2010) Down-regulation of PROS1 gene expression by 17β-estradiol via estrogen receptor α (ERα)-Sp1 interaction recruiting receptor-interacting protein 140 and the corepressor-HDAC3 complex. J. Biol. Chem. **285**, 13444-13453

[4] Yamada, M., Horiguchi, K., Umezawa, R., Hashimoto, K., Satoh, T., Ozawa, A., Shibusawa, N., Monden, T., Okada, S., Shimizu, H. and Mori, M. (2010) Troglitazone, a ligand of peroxisome proliferator-activated receptor-γ, stabilizes NUCB2 (Nesfatin) mRNA by activating the ERK1/2 pathway: isolation and characterization of the human NUCB2 gene. Endocrinology **151**, 2494-2503

[5] Fukuchi, Y., Furihata, T., Hashizume, M., Iikura, M., Chiba, K., (2010) Characterization of ribavirin uptake systems in human hepatocytes. J. Hepatol. **52**, 486-492

[6] Weigel, G., Bertalanffy, P., Wolner, E. (2002) Depletion of intracellular GTP results in nuclear factor-kappa B activation and intercellular adhesion molecule-1 expression in human endothelial cells. Mol. Pharmacol. **62**, 453-462

[7] Jones, K. A. and Peterlin, B. M. (1994) Control of RNA initiation and elongation at the HIV-1 promoter. Annu. Rev. Biochem. **63**, 717-743

[8] Fuda, N. J., Ardehali, M. B. and Lis, J. T. (2009) Defining mechanisms that regulate RNA polymerase II transcription in vivo. Nature **461**, 186-192

Conflict of interest

Authors have no conflicts of interest to declare.

Author address

E-mail: suzuki.atsuo@d.mbox.nagoya-u.ac.jp

CERVICAL CONDYLOMA ACUMINATUM SHOWS MORE PROGRESSIVE HISTOPATHOLOGICAL CHANGES THAN VULVAR CONDYLOMA ACUMINATUM

S. Mizuno[1)], K. Hashimoto[1)], K. Kawai[1)], T. Nagasaka[1)]

1) Department of Pathophysiological Laboratory Sciences, Nagoya University Graduate School of Medicine, Nagoya, Japan

Introduction

Condyloma acuminatum (CA) is a common, sexually transmitted disease caused by Human papillomavirus (HPV). So far, more than 100 HPV genotypes have been identified, 40 of which infect the genital tract. The genital-mucosal HPV types are classified on the basis of oncogenicity as low (e.g. HPV6 and 11), intermediate (e.g. HPV31, 33, 35, 51, 52 and 58) and high risk (e.g. 16 and 18) [1]. High-risk HPV is responsible for malignant tumors, especially for cervical carcinoma, whereas low-risk HPV leads to benign lesions.

Previous studies of HPV-associated lesions have shown that benign and low-grade lesions mostly contain the viral DNA as episomes. In contrast, the viral genome is integrated into the host-cell DNA in almost all high-grade lesions and cervical carcinomas [2, 3]. These observations suggest that integration of HPV into the human genome is one of the key events in the progression of neoplasia. HPV DNA integration is associated with decreased expression of HPV L1 capsid gene and increased expression of the E6 and E7 oncogene. The E6 and E7 oncoproteins of HPV cause inactivation of the tumor-suppressor proteins p53 and Rb. Rb inactivation results in the overexpression of the cyclin-dependent kinase inhibitor p16. Immunohistochemical staining for HPV-L1 capsid protein and p16 has been used for the detection of HPV infection. It has been reported in some studies that L1/p16 expression pattern could be helpful for estimating the biologic potentiality of low-grade cervical lesions [4, 5].

CA is genital warts characterized by papillomatous proliferations of the squamous epithelium. Approximately 90% of CA is related to HPV types 6 and 11. In women, CA occurs on the vulva, vagina, cervix and around the anus. Vulvar CA is commonly found but cervical CA is relatively uncommon. Although CA occurs anywhere in the genital area, few studies have examined female CA in light of its site of origin. The purpose of this study was to analyze histopathological features of cervical CA by comparison with vulvar CA. We investigated nuclear morphology, physical status of HPV DNA and protein expression (L1 and p16) in CA.

Materials and methods

Sample preparation: We obtained forty-seven formalin-fixed paraffin-embedded (FFPE) blocks composed of vulvar CA case (V-CA, n=33) and cervical CA case (CX-CA, n=14). This research was approved by the Ethics Committee of the School of Health Sciences, Nagoya University.

PCR analysis and sample selection: Genomic DNA was extracted from each sample using QIAamp® DNA Mini Kit (QIAGEN). Adequate DNA quality was established by successful PCR amplification of human ß-globin gene. HPV type-specific primers (HPV6 and HPV11) and pU-1M/pU-2R primers to amplify high-risk HPV (HPV16, 18, 31, 33, 35, 52b, and 58) DNA were used separately. Samples in which HPV6 or HPV11 were detected and high-risk HPV not detected by PCR were selected for analysis in this study (V-CA n=22, CX-CA n=12).

H&E staining and image analysis: Each section of samples selected by PCR results stained with hematoxylin and eosin (H&E). Ten digital images were taken from each H&E stained slide under high power field (HPF, x40 objective) of the microscope. The nuclear area and circularity were measured using software ImageJ 1.45s. For each sample, the mean of a nuclear area and circularity were calculated. In ImageJ 1.45s, the formula for circularity is 4π (area/perimeter^2). A value of 1.0 indicates a perfect circle, and as the value approaches 0.0, it indicates an increasingly elongated shape.

DNA in situ *hybridization for low-risk HPV: in situ* hybridization (ISH) was performed using GenPoint™ (DAKO) and DNA probe cocktails for HPV6/11 (DAKO). The HPV signal patterns in nuclei were classified as punctate, diffuse, or mixed. A punctate pattern was considered to indicate integrated HPV, and a diffuse pattern was considered to represent episomal HPV. We evaluated the physical state of HPV by classifying into five categories: I (Integrated), E (Episomal), E<I, E=I, and I<E. These categories correspond to HPV signal patterns by ISH: punctate, diffuse, the predominance of punctate, the same degree, and the predominance of diffuse, respectively.

L1, p16 immunohistochemistry: Immunohistochemical staining was performed using a L1 monoclonal antibody (clone K1H8, DAKO) and a p16 monoclonal antibody (clone E6H4, CINTec). L1 and p16 staining was scored 0, 1+, 2+, and 3+.

Statistics: Statistical analysis was performed using SPSS ver.14.0-J and MEPHAS (http://www.gen-info.osaka-u.ac.jp/MEPHAS/). Mann-Whitney test and Wilcoxon's rank-sum test were used to compare between the V-CA group and the CX-CA group. Kruskal-Wallis test with post-hoc Steel-Dwass test was applied to examine the relation between HPV DNA physical status and L1/p16 expression pattern.

Results

Nuclear morphology: The median nuclear areas were 41.71 and 39.39 μm^2 ($p=0.454$, Mann-Whitney test) and nuclear circularity values were 0.872 and 0.835 ($p<0.01$, Mann-Whitney test), respectively, in the V-CA and CX-CA group.

HPV DNA physical status: LR-HPV DNA was detected in 13 (65%) of 20 specimens of the V-CA group and all specimens (n=12) of the CX-CA group. Estimated results of HPV DNA physical status were summarized in Figure 1. Wilcoxon's rank-sum test showed a significantly different distribution ($p<0.01$) in the physical status were category between the two groups, V-CA and CX-CA. The physical status category was divided into 2 groups which defined E and I<E as Epi (Episomal) group, E=I, E<I and I as Int (Integrated) group. There was a significant difference ($p<0.01$, Fisher's exact test) between the two groups.

L1, p16 staining pattern: The expression of L1 was nuclear in superficial and intermediate cells, often with features of koilocytosis. Of the 20 specimens in the V-CA group, L1 staining score was 0 in 10 cases (50%), 1+ in 4 cases (20%), 2+ in 2 cases (10%), and 3+ in 4 cases (20%). Of the 12 specimens

in the CX-CA group, L1 staining score was 0 in 8 cases (66.67%), 1+ in 1 case (8.33%), 2+ in 1 case (8.33%), and 3+ in 2 cases (16.67%).

The expression of p16 was cytoplasmic or nuclear and cytoplasmic. Of the 20 specimens in the V-CA group, the p16 staining score was 0 in 16 cases (80%), 1+ in 4 cases (20%), 2+, and 3+ in no case. Of the 12 specimens in the CX-CA group, p16 staining score was 0 in no case, 1+ in 2 cases (16.67%), 2+ in 5 cases (41.67%) and 3+ in 5 cases (41.67%).

As for analysis of L1/p16 expression patterns, L1 staining score was classified into two groups which defined L1 staining score 0 as negative and 1+, 2+, 3+ as positive, and the p16 staining score was classified in the same way. The L1 and p16 expression, positive (+) or negative (-), could be divided into four categories as follows: L1-/p16-, L1+/p16-, L1+/p16+, L1-/p16+. L1/p16 expression in that order is shifted with increasing histological severity. Wilcoxon's rank-sum test showed a significantly different distribution ($p<0.01$) in this categories between the two groups, V-CA and CX-CA. L1-/p16- or L1+/p16- was common in the V-CX, L1+/p16+ or L1-/p16+ in the CX-CA group (Figure 2).

Relation between HPV-DNA physical status and L1/p16 expression pattern: Little information related to the relationship of between L1/p16 expression pattern and HPV DNA physical status is available. We examined the relationship of between L1/p16 expression pattern and ISH result (Figure 3). The physical status was classified into three groups: ISH negative (Neg), Epi, and Int. L1/p16 expression pattern was classified by the above-mentioned four categories. Among Neg, Epi and Int, the distribution L1/p16 expression pattern was analyzed using Kruskal-Wallis test with post-hoc Steel-Dwass test. There were significant differences between the Neg and Epi, Neg and Int, Epi and Ing group ($p<0.01$).

Discussion

Results revealed that CX-CA showed histopathologically different features from those of V-CA. Lower nuclear circularity, integrated HPV DNA and higher expression of p16 were seen in CX-CA compared with V-CA.

HPV DNA physical status evaluated by ISH was relevant to L1/p16 expression pattern. L1+/p16- or L1+/p16+ pattern was observed in the presence of episomal HPV DNA, and L1-/p16+ observed in the presence of integrated HPV DNA. All specimens with no detectable HPV DNA by ISH showed the L1-/p16- pattern. Non-detection of HPV DNA and loss of L1/p16 expression were considered consistent with a low-level or latent HPV infection. Collectively, these findings indicate that histological progression, L1/p16 expression pattern and HPV DNA physical status relate to each other.

CA is a benign tumor caused by low-risk HPV infection and considered a lower-grade lesion among HPV-associated lesions. Our results show that V-CA findings are consistent with features of a low-grade lesion, whereas CX-CA findings are not. CX-CA tended to show more progressive features, such as the abnormalities in nuclear morphology and HPV DNA integration. This suggests that the potential of integration could depend on HPV infection site. The differences between vulvar skin and cervical mucous membrane are suspected to be related to the potential of HPV DNA integration.

Conclusions

Cervical condyloma acuminatum shows more progressive histopathological changes than vulvar condyloma acuminatum. Integration of HPV DNA could depend on the HPV infection site.

References

[1] Muñoz N, Bosch FX, de Sanjosé S, et al. Epidemiologic Classification of Human Papillomavirus Types Associated with Cervical Cancer. *N Engl J Med*. 2003;348:518-527.

[2] Cooper K, Herrington CS, Stickland JE, et al. Episomal and integrated human papillomavirus in cervical neoplasia shown by non-isotopic in situ hybridisation. *J Clin Pathol*. 1991:*44*(12):990–996.

[3] Lehn H, Villa LL, Marziona F, et al. Physical state and biological activity of human papillomavirus genomes in precancerous lesions of the female genital tract. *J Gen Virol*. 1988:69:187–196.

[4] Negri G, Bellisano G, Zannoni GF, Rivasi F, Kasal, A, Vittadello F, Antoniazzi S, et al. p16 ink4a and HPV L1 immunohistochemistry is helpful for estimating the behavior of low-grade dysplastic lesions of the cervix uteri. *Am J Surg Pathol*. 2008;*32*(11):1715–1720.

[5] Hoshikawa S, Sano T, Yoshida T, Ito H, Oyama T, et al. Immunohistological analysis of HPV L1 capsid protein and p16 protein in low-grade dysplastic lesions of the uterine cervix. *Pathol Res Pract*. 2010;206(12):816–820.

Author address

E-Mail: mizuno.satomi@e.mbox.nagoya-u.ac.jp

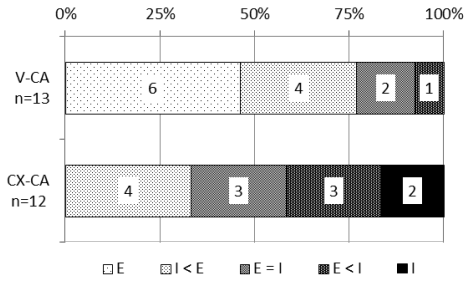

Figure 1 Distribution of HPV DNA physical status

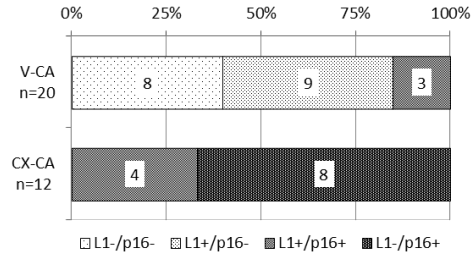

Figure 2 Distribution of L1/p16 expression pattern

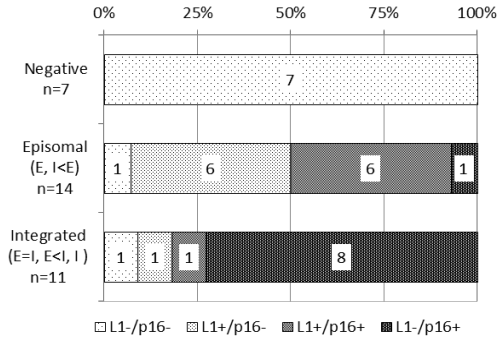

Figure 3 Relation between HPV DNA physical status and L1/p16 expression pattern

Parkin induces apoptotic cell death in TNF-α-treated cervical cancer cells

Yoonjung Cho[1], Min Ho Lee[1], Yeo Wool Kang[1], Dongsup Lee[1,2], Ki-Jong Rhee[1], Tae Ue Kim[1], Yoon Suk Kim[1]

1) Department of Biomedical Laboratory Science, College of Health Science, Yonsei University, Wonju, Korea
2) Department of Clinical Laboratory Science, Hyejeon Colleage, Hongseong, Chungcheongnam-do 350-702, Korea

Introduction

Parkin protein (parkin) was originally implicated in Parkinson's disease [1]. The parkin gene (*PARK2*) is located in chromosome 6q25.2-6q27, and loss of heterozygosity (LOH) in 6q26 was reported in ovarian, breast, hepatocellular and squamous cell lung cancers [2-4]. In addition, in a variety of cancer cells including brain, liver, colorectal, ovarian, cervical pancreas, kidney and breast cancers, alternative transcripts were found due to the deletion and duplication in *PARK2* gene [5-8]. Recent reports not only shows suppressed Parkin expression have an essential role in tumorigenesis but also suggest Parkin is a putative tumor suppresor. Overexpression of Parkin in hepatocarcinoma, glioma, lung cancer, breast cancer and colon cancer cell lines repressed growth of the cells. In glioblastoma and other cancers, Parkin overexpression results in ubiquitin mediated cyclinE degradation and subsequent cell cycle arrest. Mechanisms of Parkin for its role in tumor suppression is partly come to light but still unclear.

We mainly used HeLa, a cervical cancer cell line, for experiment, because HeLa is Parkin gene mutated and resistant to TNF-α. TNF-α is one of the cytokines secreted by immune response to suppress cancer growth in the body. However, as the cancer develops, the cancer becomes TNF-α resistant.

Our hypothesis is that Parkin expression sensitizes naturally resistant HeLa cells to TNF-α-induced tumor regression. This study will suggest a role of Parkin as a tumor suppressor in the reactions accompanied by immune reaction.

Materials and Methods

Materials

Dulbecco's modified Eagle's medium (DMEM), fetal bovine serum (FBS), penicillin-streptomycin, trypsin-EDTA, and trypan blue stain solution were from Gibco BRL. Recombinant human TNF-α was purchased from R&D Systems. DMSO and protease inhibitor cocktail were from Sigma-Aldrich. Propidium iodide (2.5 mg/ml) was purchased from BD Biosciences. Trizol reagent, random hexamer, and MMLV-RT were purchased from Invitrogen.

Cell culture and viral infection with parkin-expressing adenovirus

HeLa (human cervical adenocarcinoma cells, ATCC) cells were infected with adenoviruses as described previously [9]. In brief, cells were seeded in 6-well plates at a density of 2 x 10^5/well. After 24 h, cells were infected with 150 multiplicity of infection (M.O.I.) of parkin-expressing virus (Parkin) or mock virus (Mock) for 24 h. For dose-dependent experiments, cells were infected with 0, 19, 38, 75, and 150 M.O. of Parkin. Various concentrations of Parkin were mixed with Mock and normalized for a to tal of 150 M.O.I. per infection..

Trypan blue dye exclusion assay

Cells (2x10^5/well) were seeded in 6-well culture plates, cultured for 24 h and then infected with Parkin or Mock for an additional 24 h. The cells were then treated with TNF-α (5 ng/ml) for 24 h and the cells trypsinized, stained with trypan blue dye solution and viable cells counted on a hemocytometer.

Western blot analysis

Cells were lysed with a PBS buffer containing 1% Triton X-100 and protease inhibitor cocktail. The supernatant was collected after centrifugation and the protein concentration determined using the Lowry protein assay (Bio-Rad). Protein samples were separated by SDS-PAGE, transferred to a nitrocellulose membrane and the membrane incubated with primary antibodies overnight and then with appropriate secondary antibodies for 1 h. Bands were visualized using ECL (Thermo, Waltham, MA, USA). β-actin was used as an internal control.

RNA extraction and reverse transcriptase PCR (RT-PCR)

Total RNA was extracted from cells using Trizol. cDNA was synthesized using 2 μg of total RNA, 0.25 μg of random hexamers and 200 U of MMLV-RT. PCR was performed using 0.2 U of *Taq* polymerase (Cosmogenetech, Korea) and specific primers. GAPDH was used as an internal control. PCR products were electrophoresed on 1.5% (w/v) agarose gels containing ethidium bromide and images taken using Gel Doc (Bio-Rad).

Results

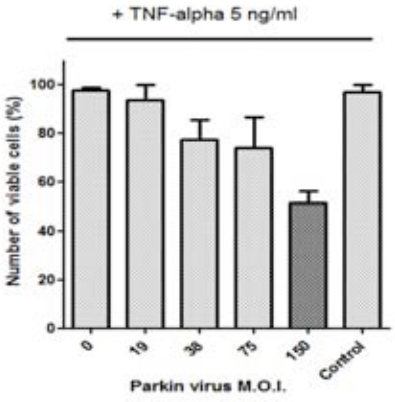

Figure 1. Expression of parkin restores susceptibility to TNF- α -induced cell death.

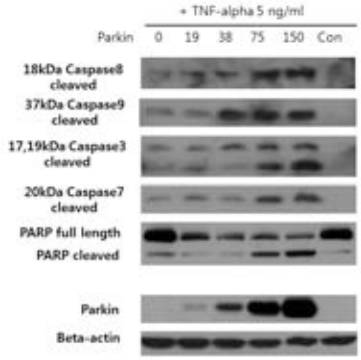

Figure 2. Caspase -8, -9, -3, -7 and Poly ADP ribose polymerase (PARP), cleaved form of which induces apoptosis, is cleaved by combination of Parkin expression and TNF-alpha treated in HeLa cells.

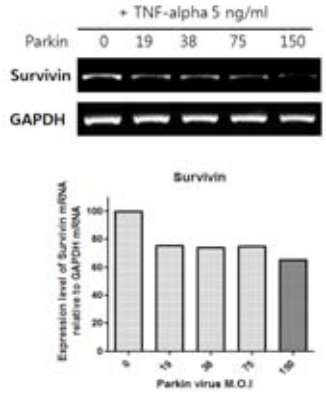

Figure 3. Parkin reduces mRNA expression of survivin in TNF-alpha treated HeLa cells.

Conclusions

Although, parkin has been proposed to be a tumor suppressor, the mechanisms by which parkin functions as a tumor suppressor are unclear. In the current study, we investigated the role of parkin in TNF-α-induced apoptosis of HeLa cells. HeLa cells are inherently resistant to TNF-α-induced cell death and also lack parkin expression. We found that ***i)*** parkin expression in HeLa cells restored TNF-α-induced cell death and ***ii)*** TNF-α-induced cell death was mediated via activation of the apoptotic pathway involving survivin, caspase-8, -9, -3,-7, and PARP.

In conclusion, we report that restoration of parkin expression in the parkin-deficient HeLa cell line restored susceptibility to TNF-α-induced cell death. Although further studies are needed to determine the exact mechanisms by which parkin expression restores TNF-α-induced cell death, we have identified signaling pathways that will provide a clue to understanding how parkin acts as a tumor suppressor.

References

[1] Shimura, H., Schlossmacher, M. G., Hattori, N., Frosch, M. P., Trockenbacher, A., Schneider, R., Mizuno, Y., Kosik, K. S. and Selkoe, D. J. (2001) Ubiquitination of a new form of alpha-synuclein by parkin from human brain: implications for Parkinson's disease. *Science* **293,** 263-269.

[2] Kong, F. M., Anscher, M. S., Washington, M. K., Killian, J. K. and Jirtle, R. L. (2000) M6P/IGF2R is mutated in squamous cell carcinoma of the lung. *Oncogene* **19,** 1572-1578.

[3] Oates, A. J., Schumaker, L. M., Jenkins, S. B., Pearce, A. A., DaCosta, S. A., Arun, B. and Ellis, M. J. (1998) The mannose 6-phosphate/insulin-like growth factor 2 receptor (M6P/IGF2R), a putative breast tumor suppressor gene. *Breast Cancer Res Treat* **47,** 269-281.

[4] Shridhar, V., Staub, J., Huntley, B., Cliby, W., Jenkins, R., Pass, H. I., Hartmann, L. and Smith, D. I. (1999) A novel region of deletion on chromosome 6q23.3 spanning less than 500 Kb in high grade invasive epithelial ovarian cancer. *Oncogene* **18,** 3913-3918.

[5] Denison, S. R., Callahan, G., Becker, N. A., Phillips, L. A. and Smith, D. I. (2003) Characterization of FRA6E and its potential role in autosomal recessive juvenile parkinsonism and ovarian cancer. *Genes Chromosomes Cancer* **38,** 40-52.

[6] Denison, S. R., Wang, F., Becker, N. A., Schule, B., Kock, N., Phillips, L. A., Klein, C. and Smith, D. I. (2003) Alterations in the common fragile site gene Parkin in ovarian and other cancers. *Oncogene* **22,** 8370-8378.

[7] Poulogiannis, G., McIntyre, R. E., Dimitriadi, M., Apps, J. R., Wilson, C. H., Ichimura, K., Luo, F., Cantley, L. C., Wyllie, A. H., Adams, D. J. and Arends, M. J. (2010) PARK2 deletions occur frequently in sporadic colorectal cancer and accelerate adenoma development in Apc mutant mice. *Proc Natl Acad Sci U S A* **107,** 15145-15150.

[8] Tay, S. P., Yeo, C. W., Chai, C., Chua, P. J., Tan, H. M., Ang, A. X., Yip, D. L., Sung, J. X., Tan, P. H., Bay, B. H., Wong, S. H., Tang, C., Tan, J. M. and Lim, K. L. (2010) Parkin enhances the expression of cyclin-dependent kinase 6 and negatively regulates the proliferation of breast cancer cells. *J Biol Chem* **285,** 29231-29238.

[9] Kim, Y. S., Patel, S. and Lee, S. J. (2006) Lack of direct role of parkin in the steady-state level and aggregation of alpha-synuclein and the clearance of pre-formed aggregates. *Exp Neurol* **197,** 538-541.

Author address

E-Mail: black5579@naver.com

Parkin induces MMP-3 expression in human cervical cancer cells

Byung Chul Jung[1], Min Ho Lee[1], Hyun-Kyung Kim[2], Ju Yeon Lee[1], In-Soo Lee[3], Ki-Jong Rhee[1], and Yoon Suk Kim[1,*]

[1]Department of Biomedical Laboratory Science, College of Health Sciences, Yonsei University, Wonju, Gangwon-do 220-710, Republic of Korea
[2]Department of Biomedical Laboratory Science, College of Natural Science, Gimcheon University, 214 Daehakro, Gimcheon City, Gyungbuk 740-704, Republic of Korea
[3]Department of Clinical Laboratory Science, Hyejeon College, Hongseong, Chungcheongnam-do, 350-702

Introduction

The parkin gene (*PARK2*) was first described in Parkinson's disease (Shimura et al., 2001). It is located on chromosome 6q25.2-6q27 which is implicated as a common fragile site (Denison et al., 2003b). Loss of heterozygosity (LOH) on chromosome 6q26 was reported in hepatocellular carcinoma, ovarian, breast, lung, and squamous cell lung cancers (Kong et al., 2000; Oates et al., 1998; Shridhar et al., 1999). Furthermore, alternative transcripts of parkin gene were found in a variety of cancers including ovarian, brain, liver, colorectal, cervical, pancreas, kidney, and breast cancer due to deletion or duplication of the gene (Denison et al., 2003a; Denison et al., 2003b; Poulogiannis et al., 2010; Tay et al., 2010; Veeriah et al., 2010; Wang et al., 2004). These reports attracted interest in the role of parkin as a putative tumor suppressor.

Matrix metalloproteases (MMP) are zinc-dependent endopeptidases that can degrade various components of the extracellular matrix thereby influencing cell proliferation, cell death, cell differentiation, cell migration, and cell–cell interactions (Van Lint and Libert, 2007). MMPs are zymogens which become enzymatically active upon after proteolytic cleavage. Active MMP-3 degrades various collagens (types II, III, IV, IX, X), proteoglycans, fibronectin, laminin, and elastin (Murphy and Nagase, 2008). In addition, MMP-3 can also activate other MMPs such as MMP-1, MMP-7, and MMP-9 (Ye et al., 1996). MMP-3 is involved in wound repair, progression of atherosclerosis, and tumor initiation (Murphy and Nagase, 2008). In general, MMPs are secreted proteins and exert its function in the extracellular environment. However, recent data suggest that MMP-3 can also act intracellularly. It has been reported that endoplasmic reticulum stress results in activation of caspase-12 which in turn activates intracellular MMP-3. Activated MMP-3 in turn directly activates caspase-3 which results in apoptosis (Choi et al., 2008; Kim et al., 2010).

In this study, we investigated the role of MMP-3 during TNF-α-mediated apoptosis in parkin expressing HeLa cells. We report that parkin induces expression of MMP-3 and inhibition of MMP-3 activity alleviates TNF-α-induced cell death in parkin expressing cells.

Materials and Methods

1. Materials

Recombinant adenoviral vector including parkin gene (Parkin virus) was produced as previously described by Kim *et al.* (Kim et al., 2006). Recombinant human TNF-α was purchased from R&D System (Minneapolis, USA). Ro 31-7549, PD 98059, Ly 294002, SB 203580, GW 5074, JNK inhibitor II, and N-Isobutyl-N-(4-methoxyphenylsulfonyl)-glycylhydroxamic Acid (NNGH) were purchased from Calbiochem (Darmstadt, Germany). BAY 11-7085 was purchased from Enzo life science (New York, USA). U73122 was purchased from Cayman (Michigan, USA).

2. Cell lines and cell culture

HeLa (Human cervical adenocarcinoma cells, ATCC) was grown in Dulbecco's modified Eagle's medium (DMEM) (Gibco BRL, Carlsbad, USA) supplemented with 10% fetal bovine serum (FBS) (Gibco BRL, Carlsbad, USA) and streptomycin-penicillin (Gibco BRL, Carlsbad, USA). Cells were maintained at 37℃ in humidified atmosphere with 5% CO_2.

3. Parkin gene expression

HeLa cells (2 x 10^5) were seeded into each well of a 6-well plate and 24 h later infected with different concentrations of Parkin virus and Mock virus in serum-free DMEM. After an additional 90 min 10% FBS-DMEM was added to each well. In Parkin virus dose-dependent experiments, cells were infected with Parkin virus at different multiplicity of infection (M.O.I.)(0, 25, 50, 100, 200). To compensate for the effect of the viral vector Mock virus was added with the Parkin virus to maintain equal concentration of 200 M.O.I. A non-infected group was added as a negative control.

4. Trypan blue dye exclusion assay

The cell culture medium was removed and treated with trypsin-EDTA (Gibco BRL, Carlsbad, USA) for 2 min. Cells were dislodged and an equal volume of cell suspension mixed with 0.4% trypan blue stain solution (Gibco BRL, Carlsbad, USA). Viable cells were enumerated using a hematocytometer (Marienfeld, Lauda-Königshofen, Germany).

5. RT-PCR (Reverse transcriptase - polymerase chain reaction)

Total RNA was extracted from cultured cells using Trizol reagent (Invitrogen, New York, USA) according to the manufacturer's instructions. cDNA was synthesized by reverse transcription with 2 μg total RNA, 0.25 μg of random hexamer (Invitrogen, New York, USA) and 200 U of Moloney Murine Leukemia Virus-Reverse Transcriptase (MMLV-RT; Invitrogen, New York, USA) for 50 min at 37℃ and 15 min at 70℃. Subsequent PCR amplification using 0.2 U of *Taq* polymerase (Cosmogenetech, Seoul, Korea) was performed in a thermocycler using specific primers. The sequences of the PCR primers are as follows: 5'-ggc cag gga tta atg gag at-3' (forward) and 5'-gct gac agc atc aaa gga ca-3' (reverse) for MMP-3 and 5'-cgg gaa gct tgt cat caa tgg-3' (forward) and 5'-ggc agt gat ggc atg gac tg-3' (reverse) for GAPDH. PCR products were electrophoresed on 1.5% agarose gels, stained for 10 min with ethidium bromide and destained for 20 min. Product size were determined by comparing to a 100 bp DNA ladder marker (Bioprince, Georgia, USA). The intensity of each band was quantitated using a Gel Doc (Bio-Rad, California, USA).

Results

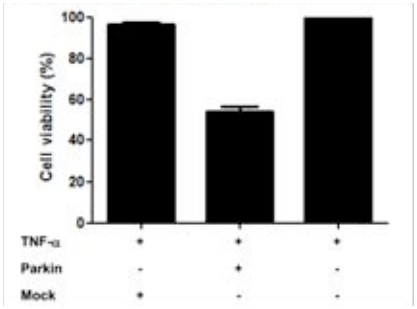

Figure 1. Parkin expression restores susceptibility to TNF-α-induced death in HeLa cells.
HeLa cells were infected with either Parkin virus or Mock virus (200 M.O.I.) for 24 h and then treated with TNF-α (5 ng/ml) for 24 h. Viable cells were enumerated by trypan blue dye exclusion assay. The number of viable cells in the non-infected group was set as 100 %. Data are from three independent experiments.

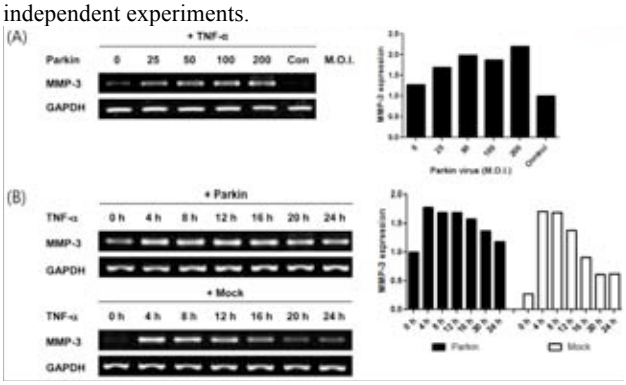

Figure 2. Parkin induces prolonged expression of MMP-3 in TNF-α-treated HeLa cells.

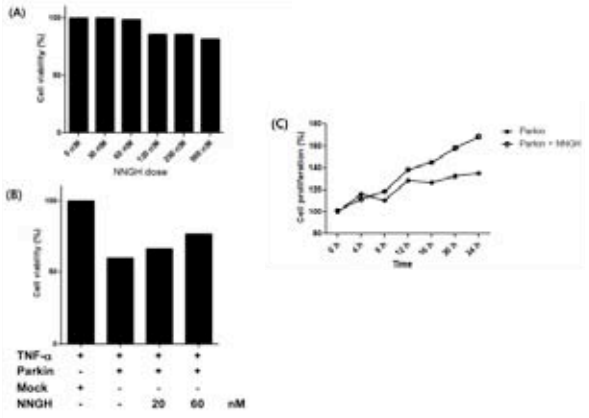

Figure 3. Parkin expression-induced reduction of cell viability in TNF-α-stimulated HeLa cells was partially recovered by MMP-3 specific inhibitor.

Discussion

Many studies suggest a tumor suppressive role of Parkin but the mechanism by which it acts is still unclear. In this study, we investigated the implication of MMP-3 in parkin-induced TNF-α-treated HeLa cell death. We found that i) parkin induces expression of MMP-3, and ii) inhibition of MMP-3 activity alleviates Parkin+TNF-α-treated HeLa cell death.

TNF-α is a potent activator of apoptosis and a defect in the apoptotic pathway contributes to uncontrolled cell proliferation resulting in cancer development (Balkwill, 2009). Caspases play a central role in the transduction of TNF-α-induced apoptotic signals. The initiator caspases, caspase-8 (mitochondria independent) and caspase-9 (mitochondria dependent) and the effector caspases, caspase-3 and caspase-7 are crucial signaling molecules involved in this apoptotic pathway (Fesik and Shi, 2001). A recent study reported that MMP-3 activates caspase-3 leading to neuronal apoptosis (Choi et al., 2008). Therefore, in the current study we investigated the expression of MMP-3 during TNF-α-induced cell death in parkin expressing HeLa cells. In this study, we showed that expression of parkin in HeLa cells induces a slight increase in MMP-3 expression which increases further when treated with TNF−α (Fig. 2A). Our results imply parkin affects up-regulation of MMP-3 in TNF-α−treated HeLa cells. In addition, we found that a positive correlation between increase in MMP-3 activity and TNF-α-induced cell death in parkin-expressing HeLa cells (Fig. 3B, C).

Interestingly, we found a dramatic but short-lived increase in MMP-3 expression when HeLa cells were infected with the Mock virus and then treated with TNF-α (Fig. 2B). One possibility is that infection with the adenovirus itself is sufficient to induce a transient increase in MMP-3 expression. We are unaware of any reports to this effect. However, a recent report showed that introduction of Poly (I:C), a synthetic analog of viral double-stranded RNA, into corneal fibroblasts upregulated MMP-3 (Kimura et al., 2010). The adenovirus vector that we used in this study is a double-stranded DNA virus (Philipson et al., 1975). It remains to be seen whether dsDNA is sufficient to induce MMP-3 expression.

Moreover, the interaction between parkin and MMP-3 with other apoptotic proteins remains to be determined. Further studies seem to be needed to elucidate mechanism(s) by which MMP-3 plays a role in Parkin+TNF-α-induced cell death and it would be interesting to determine if other MMPs are also regulated by Parkin.

References

Agirre X, Roman-Gomez J, et al. Abnormal methylation of the common PARK2 and PACRG promoter is associated with downregulation of gene expression in acute lymphoblastic leukemia and chronic myeloid leukemia. Int J Cancer. 2006. 118: 1945-1953.

Balkwill F. Tumour necrosis factor and cancer. Nat Rev Cancer. 2009. 9: 361-371.

Choi D H, Kim E M, et al. A novel intracellular role of matrix metalloproteinase-3 during apoptosis of dopaminergic cells. J Neurochem. 2008. 106: 405-415.

Denison S R, Callahan G, et al. Characterization of FRA6E and its potential role in autosomal recessive juvenile parkinsonism and ovarian cancer. Genes Chromosomes Cancer. 2003a. 38: 40-52.

Shimura H, Schlossmacher M G, et al. Ubiquitination of a new form of alpha-synuclein by parkin from human brain: implications for Parkinson's disease. Science. 2001. 293: 263-269.

Induction of the IL-2-independent growth by KRAS G12A mutation

N. Mizutani[1)], T.Murate[1)]

1) Department of Pathophysiological Laboratory Sciences, Nagoya University Graduate School of Medicine, Nagoya, Japan

Introduction

MOTN-1 and PLT-2 are human T-cell large granular lymphocyte (T-LGL) leukemia cell lines derived from the same patient at defferent disease stage.[1),2)] MOTN-1 was established at the indolent and chronic stage, and is IL-2 dependent, whereas PLT-2 was established from the aggresssive and termnal stage and is IL-2 independent. Karyotype analysis of the two cell lines showed that PLT-2 cells retain the basic abnormalities observed in MOTN-1 cells. In the present study, we analyzed the signal transduction pathway of these two cell lines with or without IL-2 treatment, and found that the constitutively active ERK pathway is important for the survival of PLT-2. We detected *KRAS* mutation in parallel with the increased Ras activity of PLT-2 but not MOTN-1 cells.

Materials and Methods

Cells and reagents

MOTN-1 and PLT-2 cells were derived from Kochi University School of Medicine. MOTN-1 cells were cultured in 10% FCS and IL-2 (100 U/ml) in RPMI1640. IL-15 was purchased from Peprotech (Rocky Hill, NJ, USA). Cell signaling inhibitors: SB203580, was purchased from Wako (Osaka, Japan), JAK Inhibitor I was from Merck chemicals (Darmstadt, Germany), LY294002, PD90859, and U0126 were from Cell Signaling Technology (Beverly, MA, USA) respectively. NIH3T3 cells and its transfectants were cultured in 5% FCS in DMEM.

Cell viability

Viable cell number was counted by the trypan blue dye exclusion method.

Western blotting

Anti-Bcl-2 antibody, anti-Bcl-X_L antibody (BD Transduction Laboratories, Franklin Lakes, NJ, USA), anti-p15 antibody, anti-p27 antibody, anti-cyclin D3 antibody, anti-p-STAT3 antibody, anti-cyclin dependent kinase (CDK) 4 and 6 antibodies (Cell Signaling), anti-STAT3 antibody, anti-STAT5 antibody, anti-p-STAT5 antibody (Sigma), anti-Akt antibody, anti-p-Akt antibody, anti-ERK 1/2 antibody, anti-p-ERK 1/2 antibody (Santa Cruz Biotechnology, Santa Cruz, CA, USA), and anti-β-actin antibody (Bio vision, Milpitas, CA, USA).

Ras activity assay

Ras activity was measured using an Active Ras Pull-Down and Detection kit (Thermo Scientific, Billerica, MA, USA) according to the manufacturer's instructions.

MAPK/ERK pathway activation

PathDetect Elk1 trans-reporting system (Agilent Technologies, La Jolla, CA, USA) was used to determine the activated state of the MAPK/ERK pathway according to the manufacturer's manual.

RAS and PTPN11 mutation study

N, *K* and *HRAS* and *PTPN11* mutations were analyzed by RT-PCR followed by direct sequencing. Reported hot spots of *RAS* (corresponding to the amino acid 12, 13 and 61) were surveyed. The whole coding sequence of *PTPN11* was analyzed.

Transfection and colony formation of NIH3T3

NIH3T3 cells were transfected with pcDNA 3.1 expression vectors containing wild-type *KRAS*, *KRAS* G12A and *KRAS* G12V, respectively. After G418 selection, suitable subclones were selected by determining respective phosphorylated ERK level. In order to directly demonstrate the growth advantage of NIH3T3 cells transfected with mutated *KRAS*, we performed the colony formation assay. Through preliminary experiments, the suitable initial cell density for plating and the culture period were determined. Briefly, stably transfected-NIH3T3 cells were placed in a tissue culture plate (35 mm diameter) in triplicate. After 10 days, tissue culture plates were stained with May-Giemsa staining dye. Colony number was counted under the inverted microscope.

KRAS Eexpression vectors and transfection for MOTN-1

KRAS wild type, *KRAS* G12V, and *KRAS* G12A were inserted into the suitable multi-cloning site of Original MSCV-GFP vector. After obtaining culture supernatant containing retroviruses, MOTN-1 cells were transfected with culture supernatant containing MSCV-GFP-*KRAS* (wild, G12A, and G12V) or MSCV-GFP (as the mock vector). Cells were sorted by FACS according to their GFP fluorescent intensity. Strongly positive cells were collected and used for further analysis.

Results

Difference of cytokine dependence between MOTN-1 and PLT-2

IL-2 and IL-15 receptors are composed of α, β and γ subunits, and share β and γ chains. Consistently, MOTN-1 proliferated with either IL-2 or IL-15 but stopped proliferation by depleting IL-2 or IL-15. However, PLT-2 did not require either of these cytokines for proliferation.

Status of signaling pathway and Ras analysis

Examination of apoptosis- and cell cycle-related proteins revealed that p15 and p27 were increased after depletion of IL-2 in MOTN-1, whereas cyclin D3 and CDK6 did not show significant changes by IL-2 depletion. In MOTN-1, activated STAT3 and STAT5 were observed in IL-2 (+) cells. STAT activation was also observed in IL-2 (+) but not in IL-2 (-) PLT-2, suggesting that JAK2/STAT pathway was not involved in its IL-2 independent growth.

However, activated ERK pathway was observed in PLT-2 cells as compared with that of MOTN-1. AKT signaling did not show significant change between MOTN-1 and PLT-2 regardless of cytokine treatment. Increased Ras activity of PLT-2 parallels ERK activation compared with MOTN-1. Direct sequence of *N, K* and *HRAS* revealed *KRAS* G12A mutation in PLT-2 but not in MOTN-1. Our preliminary analysis using allele-specific PCR showed that this mutation was only present in a population of the original leukemia cell DNA in the aggressive phase.

In Noonan syndrome and JMML, mutations of *PTPN11* that encode SHP2, an SH-2 domain containing tyrosine phosphatase, have been reported, and its mutation leads to the enhanced Ras/MEK signaling.[3)] However, *PTPN11* mutation was not detected in PLT-2. Moreover, MEK inhibitor, PD98059 and U0126, and farnesylation inhibitor FTI277, inhibited cell growth of PLT-2 cells. PI3K inhibitor, LY294002, but not p38 inhibitor, SB203580 and JAK inhibitor I, showed some inhibition. These results demonstrate the importance of Ras/MAPK signaling pathway of PLT-2 cell proliferation.

Overexpression of KRAS mutattions

In order to examine the role of *KRAS* G12A found in PLT-2, we transfected various *KRAS* expression vectors into NIH3T3 and MOTN-1 cells. The effect of *KRAS* G12V, a *KRAS* common mutation observed in various cancer cells, was also analyzed. High ERK activation was observed in *KRAS* G12A and G12V transfectants of NIH3T3 as compared with mock- and wild-type *KRAS* expressed cells, respectively. Enhanced Ras activity of *KRAS* G12A and G12V leading to activation of ERK pathway was also demonstrated using Elk-1 trans-reporting system. Colony formation of respective *KRAS* transfected-NIH3T3, suggesting the significantly enhanced colony formation of *KRAS* G12A and G12V but not of wild-type *KRAS* NIH3T3 .

ERK activation by mutated *KRAS* was also observed in *KRAS* retrovirus-transfected MOTN-1. High Ras activity was observed in mutated *KRAS*-transfectants. *KRAS* G12V and *KRAS* G12A exhibited higher proliferation in the absence of IL-2 and resistance against both serum and IL-2 depletion during our observation period.

Discussion

LGL leukemia features a clonal expansion of antigen-primed, competent, cytotoxic T lymphocytes. IL-15, IL-2 and PDGF are included in the recent network model of survival signaling of this leukemia.[4] IL-2 and IL-15 share their β and γ chains, and IL-2 and IL-15 α receptor subunits are co-expressed in T cells.[5] Our results indicate that the proliferation signals of MOTN-1 utilized these common chains.

Comparison between MOTN-1 and PLT-2 cultured with or without IL-2 revealed increased levels of cell cycle regulators, p27 and p15, in MOTN-1 by IL-2 depletion, which is consistent with the growth arrest of MOTN-1. However, we could not detect the change of cyclins, CDK, and apoptosis-related proteins of MOTN-1 under our experimental conditions. Apoptosis related proteins (Bcl-2, Bcl-xL, Bax and Bad) also showed no significant changes after IL-2 depletion. These data might be related with the fact that IL-2-depleted MOTN-1 cells were relatively resistant to apoptosis during the short-term observation period.

Considering a similar TCR rearrangement pattern between MOTN-1 and PLT-2 and shared chromosome abnormalities,[6,7] PLT-2 was thought to be derived from MOTN-1 or at least maintain the basic cellular characteristics. Our analysis revealed that IL-2-independent growth of PLT-2 was at least partially due to the constitutive activation of the MAPK/ERK pathway but not the activated AKT and STAT pathway. MEK inhibitor or farnesylation inhibitor inhibited cell growth of PLT-2 cells. The coupling of ERK and activated Ras has been reported previously in lymphoproliferative disease of granular lymphocyte.[6]

Enhanced Ras activity of PLT-2 was thought to be due to *KRAS* G12A mutation, because no *HRAS*, *NRAS* or *PTPN11* mutation was observed. The possibility of autocrine production of IL-2 or IL-15 was less likely, because culture medium of PLT-2 did not sustain cell proliferation of MOTN-1. Ras pathway is important for survival, proliferation, senescence and differentiation. Ras activation causes Raf recruitment and activation by phosphorylation, followed by activation of the MEK and ERK sequentially. Mutation of Ras family (HRas, NRas and KRas) induced abnormal cellular signaling, deregulation of gene expression and oncogenensis.[7] Oncogenic *KRAS* mutation initiates leukemia in hematopoietic stem cells.[8]

Among three *KRAS* mutation hot spots, *KRAS* codon 12 mutation induces higher resistance to apoptosis and predisposition to anchorage-independent growth than codon 13 mutation.[9] *KRAS* G12A is relatively rare in clinical cancer samples and cell lines,[10] and the transformation activity of *KRAS* G12A remains to be disclosed.[11] Our results showed increased Ras activity and enhanced ERK signaling by *KRAS* G12A was clearly shown using transfected NIH3T3 cells and MOTN-1 cells. The analysis of relapsed childhood acute lymphoblastic leukemia revealed that *KRAS* mutation was observed only in relapsed patients.[12] Such patients with *KRAS* mutation profit from MEK inhibitors.[13] *RAS* mutation analysis of CMML patients suggests that *RAS* mutation is a secondary event that contributes to the expansion of s malignant clone with proliferative advantage.[14] PLT-2 is assumed to be from patient leukemia cells in the aggressive phase, which are transformed from cells in the chronic phase. Our preliminary results using allele-specific PCR showed that this mutation was present in the patient blast of the aggressive phase but not occurred during the *in vitro* culture process. Thus, *KRAS* mutation of this patient is a late event during his LGL leukemia progression.

The frequency of *KRAS* mutation in LGL leukemia remained to be determined previously. The mechanism of the cytokine-independent growth of LGL clinical samples has not been disclosed fully. Thus, the clinical significance of our observation is not clear enough at the moment and the future analysis of LGL leukemia samples is warranted. Recently, the comprehensive dynamical and structural analysis of a network model of this disease has revealed several key components important for the leukemogenesis and the value of importance of Ras as the network component in T-LGL leukemia has been shown.[4,15]

In the present study, *KRAS* G12V as well G12A induced ERK1 and ERK2 activation and anchorage-independent growth in NIH3T3 cells and the growth advantage of mutated *KRAS*-transfected MOTN-1 cells in IL-2 depleted medium was clearly shown. However, *KRAS* G12A mutation has been reported in IL-2-dependent KHYG-1 cell lines.[16] Ras-overexpressed factor-dependent FDC-P1 cells exhibit resistance to apoptotic cell death by cytokine depletion,[17] and *RAS* mutation induces increased anti-apoptosis in some models.[18] Thus, *RAS* mutation is necessary but not always sufficient for cytokine-independent growth. Other factors such as c-myc cannot be ruled out to confer IL-2 independent growth to PLT-2 cells.

Taken together, we found that *KRAS* G12A mutation is important for IL-2- independent proliferation, which occurred during disease progression of the patient from whom these two cell lines were established.

Reference

1) Gilliland DG. *Semin Hematol,* 2002; 39**:** 6-11.
2) Matsuo Y. *Leuk Res,* 2002; 26**:** 873-879.
3) Chan G. *Cancer Metastasis Rev,* 2008; 27**:** 179-192.
4) Zhang R. *Proc Natl Acad Sci USA,* 2008; 105**:** 16308-16313.
5) Vamosi G. *Proc Natl Acad Sci USA,* 2004; 101**:** 11082-11087.
6) Epling-Burnette PK. *Oncogene,* 2004; 23**:** 9220-9229.
7) Ulku AS. *Cancer Treat Res,* 2003; 115**:** 189-208.
8) Zhang J. *Blood,* 2009; 113**:** 1304-1314.
9) Guerrero S. *Cancer Res,* 2000; 60**:** 6750-6756.
10) Deschoolmeester V. *Br J Cancer,* 2010; 103**:** 1627-1636.
11) Seeburg PH. *Nature,* 1984; 312**:** 71-75.
12) Davidsson J. *Leukemia,* 2010; 24**:** 924-931.
13) Kiessling MK. *Blood,* 2011; 117**:** 2433-2440.
14) Ricci C. *Clin Cancer Res,* 2010; 16**:** 2246-2256.
15) Saadatpour A. *PLoS Comput Biol,* 2011; 7**:** e1002267.
16) Choi YL. *Leuk Res,* 2005; 29**:** 943-949.
17) McGlynn AP. *Leuk Res,* 2000; 24**:** 47-54.
18) Shinjyo T. *Tohoku J Exp Med,* 2008; 216**:** 25-34.

Author address

E-Mail:mizuani.naoki@e.mbox.nagoya-u.ac.jp

Changes of Matrix Metalloproteinases (MMPs) Expression in Triglyceride Treated Macrophages.

Jaewon Lim[1], Yoonjung Cho[1], Byung Chul Jung[1], Hyun-Kyung Kim[1,2], Yeo Wool Kang[1], Ki-Jong Rhee[1], Tae Ue Kim[1] and Yoon Suk Kim[1]

[1]Department of Biomedical Laboratory Science, College of Health Sciences, Yonsei University, Wonju 220-710, Korea
[2]Department of Biomedical Laboratory Science, College of Natural Science, Gimcheon University, Gimcheon 740-704, Korea

Introduction

Triglyceride (TG) is known to be associated with inflammatory disease including atherosclerosis. Recently, it has been reported that triglyceride is an independent risk factor in atherogenesis. TG has been proposed to induce cell death of macrophage or foam cell, resulting in increased inflammatory reactions in plagues. Moreover, it has been reported that matrix metalloproteinases (MMPs) have an important role in a variety of inflammatory reactions. MMPs are zinc-dependent endopeptidases which digest extracellular matrix (ECM) in normal processes. In addition, dysregulation of MMPs leads to destruction of connective tissue and various pathological inflammatory conditions. Depending on their substrate specificity and domain structure, MMPs are divided into six subclasses including collagenases, gelatinases, stromelyisins, matrilysins, membrane-type MMPs and others. Under physiological conditions, expression of MMPs is tightly regulated on mRNA level by a variety of growth factors, cytokines, chemokines and contact to the ECM. In this study, changes in expression of MMPs were investigated during monocyte differentiation into macrophages, and when the macrophages ingest TG after differentiation.

Materials and Methods

Inhibitors

Phorbol 12-myristate 13-acetate (PMA) was purchased from Sigma-Aldrich (St. Louis, MO, USA). TG was provided by B. Braun Melsungen AG (Melsungen, Germany). TRIzol for RNA isolation were obtained from Invitrogen (Carlsbad, CA, USA). Specific inhibitors of classical PKC (RO-31-7549), MEK1 (PD 98059), PI3-K (Ly 294002), p38 MAPK (SB 203580) and cRAF-1 kinase (GW 5074) were purchased from Calbiochem (Darmstadt, Germany). Specific inhibitor of NF-κB (BAY 11-7085) was purchased from Enzo life science (New York, NY, USA). Specific inhibitor of PLC (U 73122) was purchased from Cayman (Ann Arbor, MI, USA). Dimethyl sulfoxide (DMSO) was obtained from Sigma-Aldrich (St. Louis, MO, USA).

Cell culture and treatments

The human monocytoid THP-1 leukemia cell line was cultured in RPMI medium 1640 supplemented with 2 mM L-glutamine, 100 U/ml penicillin, 100 μg/ml streptomycin and 10% fetal bovine serum (FBS) at 37℃ under 5% CO_2. THP-1 cells were seeded at a density of 1×10^6 cells/well in 6-well plates and treated with the indicated concentrations of PMA to induce differentiation into macrophages. Differentiated macrophages were incubated with the indicated concentrations of TG.

mRNA extraction and semi-quantitative reverse transcriptase PCR (RT-PCR)

Total RNA was extracted from cultured THP-1 cells and PMA-differentiated THP-1 cells by using TRIzol reagent according to the manufacturer's instructions. cDNA was synthesized by reverse transcription with 2 μg total RNA, 0.25 μg of random hexamer (Invitrogen) and 200 unit of Murine Molony Leukemia Virus Reverse Transcriptase (MMLV-RT; Invitrogen) for 10min at 25°C, 50min at 37°C and 15min at 70°C. Diluted reverse-transcribed cDNA was used for subsequent 20 μl PCR amplification. PCR amplification using Prime Taq premix PCR kit (Genet Bio, Chungnam, Korea) was performed in a thermocycler (Applied Biosystems, New York, NY, USA) for 25 ~ 40 cycles using MMPs primers for MMP-1, MMP-8, MMP-3, MMP-10, MMP-12, MMP-19, MMP-2, MMP-9 and MMP-7. The levels of gene expression were normalized against GAP-DH. PCR products were electrophoresed on 2.0% (w/v) agarose gels containing 0.5 μg/ml ethidium bromide (Et-Br), and the sizes of the products determined by comparison to 100 bp DNA ladder marker (Intron, Gyeonggi, Korea). Gel images were taken using Gel-Doc (Bio-Rad, Hercules, CA, USA). The intensity of each band amplified by RT-PCR was analyzed using Image Lab (version 2.0, Bio-Rad) and normalized to GAP-DH in corresponding samples.

Results

Increased expression of MMPs during PMA induced differentiation of THP-1 cells

PMA, which promotes differentiation of monocytes, is known to stimulate secretion of MMP-1, -3, -7, -9, -12 and -14 in macrophages. Almost all MMPs showed increased expression during differentiation of monocyte into macrophage except for MMP-2 **(Fig 1)**. However, the initiation of expression was different for each MMP.

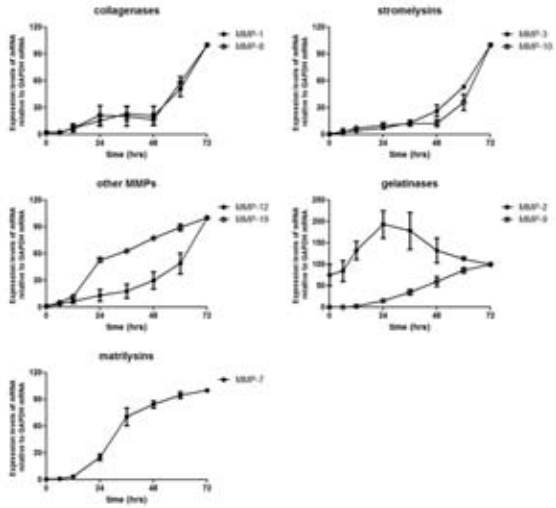

Fig 1. Time-dependent expression of MMPs during PMA induced differentiation of THP-1 cells.

PKC is not involved in PMA-induced increase of MMPs expression

The THP-1 cell lines were treated with PMA which is PKC activator to induce differentiation into macrophages. To elucidate the mechanism by which PMA treatment affects expression of MMPs, we examined the PKC signaling pathway associated with PMA-stimulated induction of MMPs **(Fig 2)**. Interestingly, expression pattern of MMPs was not changed by RO-31-7549 (an inhibitor of classic PKC). The results showed that PKC was not associated with PMA-dependent increased mRNA expression of MMPs.

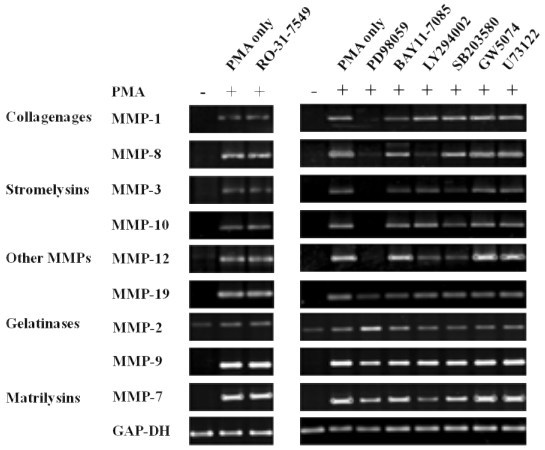

Fig 2. MEK1-mediated up-regulation of MMPs during PMA-induced differentiation of THP-1 cells.

PMA-dependent increased mRNA expression of MMPs was mediated by MEK-1

To elucidate the mechanism by which PMA treatment affects expression of MMPs, we examined the various signaling pathway molecules associated with PMA-stimulated induction of MMPs. Treatment with GW 5074 (an inhibitor of cRAF-1 kinase) or U 73122 (an inhibitor of PLC) did not influence PMA-mediated expression of MMPs. In contrast, treatment with PD 98059 (an inhibitor of MEK-1) almost completely blocked PMA-mediated expression of MMPs except for MMP-2. PD 98059 had slight negative effects on PMA-mediated expression of MMP-19, -9 and -7 **(Fig 2)**. These results suggested that the signal transduction molecule, MEK-1, was involved in the increased expression of MMPs during macrophage differentiation.

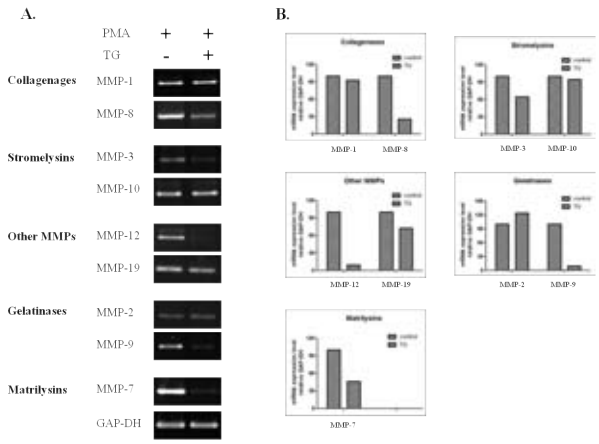

Fig 3. TG induced reduction of MMPs expression in PMA differentiated THP-1 macrophage cells.

TG induced reduction of MMPs expression in PMA differentiated THP-1 macrophage cells

To investigate the modulation of MMPs expression by accumulation of TG in differentiated THP-1 cells, THP-1 cells were treated with 200 nM PMA for 48 h to induce differentiation into macrophages and then treated with 1mg/ml TG for the last 24 h. TG treatment of differentiated macrophages resulted in inhibition of expression of most MMPs except for MMP-1, -10, and -2. The most dramatic decreased expression was observed for MMP-8, -12 and -9. However, expression of MMP-2 increased slightly. The results showed that TG was decreased expression of most MMPs in differentiated THP-1 cells.

Discussion

MMPs was known to be expressed only in low level in peripheral blood monocytes. When monocytes contact with the ECM, expression level of MMPs is activated and extracellular secretion of MMPs is increased. These phenomenon increased degradation of ECM, therefore play a important role of cell migration in tissue. In this study, we showed that expression level of most MMPs increased during differentiation of monocyte into macrophage, except for MMP-2. These results suggest that increased expression level of MMPs during macrophage differentiation helps differentiated monocyte invasion in tissue of inflammatory site. In addition, MEK-1 inhibtor decreased the rising of expression level of MMPs. These results showed that the signal transduction molecule, MEK-1, mediated expression of MMPs during macrophage differentiation. Therefore, These results suggest that developments of selective inhibitory drugs of MEK-1 would be helpful in effect of reduce inflammation response by cell migration of macrophage. TG treatment in differentiated THP-1 cell reduced expression of several MMPs. Independent of MMPs subtypes, TG accumulation changed expression level of MMPs in differentiated THP-1 cells. In particular, expression level of MMP-8, -12 and -9 was dramatically decreased. These results show that TG accumulation in differentiated macrophage reduced expression of MMPs. One of the suggestion is that reduction of MMPs maybe leads to partially blocked cell migration of macrophage in inflammatory site and associated weakening of inflammation response. Another suggestion is that these reponses increased plaque formation and inflammation response by decreased escaping of TG uptaked macrophage in atherosclerotic regions. However, more study should be investigated to prove these hypotheses. These results provide basic information for studying MMPs expression during macrophage differentiation and foundation for studies of role of MMP in triglyceride mediated inflammatory diseases.

References

[1] Andrew CN. Metalloproteinases expression in monocytes and macrophages and its relationship to atherosclerotic plaque instability. *Arterioscler Thromb Vasc Biol*. 2008. 28:2108-2114

[2] Bar-Or A, Nuttall RK, Duddy M, Alter A, Kim HJ, Ifergan I, Pennington CJ, Bourgoin P, Edwards DR, Yong VW. Analyses of all matrix metalloproteinase members in leukocytes emphasize monocytes as major inflammatory mediators in multiple sclerosis. *Brain*. 2003. 126: 2738–2749

[3] Moreno MJ, Falk E, Palacios IF, Newell JB, Fuster V, Fallon JT. Macrophage infiltration in acute coronary syndromes. Implications for plaque rupture. *Circulation*. 1994. 90:775-778

[4] Stamenkovic I. Extracellular matrix remodelling: the role of matrix metalloproteinases. *J Pathol*. 2003. 200(4):448-464